

# Coherent nonlinear Thomson scattering of Laguerre - Gauss beams on an electron sheet

Petru-Vlad Toma <sup>1,2</sup> Andrei Cristian Opinca,<sup>2</sup> Virgil Baran <sup>2,3</sup> and Madalina Boca <sup>2,\*</sup>

<sup>1</sup>*Center for Advanced Laser Technologies, National Institute for Laser, Plasma and Radiation Physics, Magurele, Romania*

<sup>2</sup>*University of Bucharest, Department of Physics, Magurele, Romania*

<sup>3</sup>*Academy of Romanian Scientists, Strada Ilfov 3, Sector 5, 050044, Bucharest, Romania*

(Dated: August 9, 2024)

We present a study of the scattering of a monochromatic helical laser beam, described by a Laguerre-Gauss solution of the Maxwell equations, on an electron sheet, initially at rest in the focal plane of the laser; the interaction is described in the framework of a local plane wave approximation. We calculate the scattered electromagnetic field observed in an arbitrary point at a large distance from the laser focal spot, by adding coherently the contributions of each electron in the electron sheet. Due to the interference effects, the radiation is emitted only into the forward direction, within a narrow cone, and it has a spatial structure that we analyze theoretically and numerically. For circularly polarized incident fields, the structure is also helical, with a helical index which depends on the helical index of the incident radiation and the harmonic order. These structures can be observed experimentally, as each harmonic order is emitted with a different frequency, and within cones of different opening angles. Our findings are in agreement with experimental results in the literature which demonstrate the generation of OAM carrying photons by radiation scattering on electrons.

*Introduction.* Starting from the experimental and theoretical results presented in [1, 2], demonstrating the generation of OAM-carrying photons in the laser electron interaction, we present here a study of the coherent nonlinear Thomson scattering of Laguerre Gauss modes on a statistical ensemble of electrons, modelled as an electron sheet.

Non-linear Thomson scattering is the scattering of the classical electromagnetic field on free electrons. Early studies such as [3–9] presented the field scattered by a single electron calculated in the long distance approximation; a detailed review of the literature can be found, for example, in [10]. The angular momentum of the field emitted by a single particle was discussed in the papers by Bordovitsyn et al [11], Katoh et al [12], Epp and Guselnikova [13, 14]. The topic of orbital angular momentum of the scattered light is especially important in the context of many applications of OAM carrying fields [15]; Taira et al [2] studied the spatial structure of the gamma rays emitted in nonlinear inverse Thomson scattering of circularly polarized light on a single electron, and found vortices, with a helical phase structure  $e^{i(N-1)\Phi}$ , where  $N$  is the harmonic order. Other works that studied the structure of the radiation emitted in the non-linear Thomson process are [16–19].

In the problem of scattering of electrons on structured fields, such as focused pulses or more complex, OAM carrying beams, the initial position of the particle determines the properties of the radiation emitted; several studies took into account not just the scattering on a single electron, but on a statistical ensemble of electron

distributed in the focal spot of the laser. Vais and Bychenkov [20] studied the incoherent non-linear Thomson scattering of a tightly focused relativistically intense laser pulse by an ensemble of particles. Another study of incoherent scattering of radiation of a Laguerre-Gauss laser beam on electrons is presented in [21].

In the model of incoherent scattering, the energy radiated by each particle is simply added, without taking into account the interference effects of the electromagnetic field emitted from different points in the electron distribution. On the other hand, the model of coherent scattering, taking the interference into account was used in studies of Thomson scattering on plasma, (see [22] and the references therein).

The experimental observation of a structured field emitted coherently by an ensemble of electrons was reported as early as 2013 by Hensing et al [1]; in their work, a Gaussian pulse was used, which was converted to an OAM mode in the interaction with a helically modulated electron-beam.

We analyze the scattering of a Laguerre-Gauss laser beam on a statistical ensemble of electrons; in this case, the spatial structure of the incident laser beam realizes the modulation of the electron distribution. The temporal Fourier transform of the field emitted by each point of the sheet is calculated and then we take the *coherent* sum over the entire distribution for each harmonic. We show that the interference effects lead to a vortex field, as that predicted by Taira [2], but with a more complex expression of the phase, which in our case, for the  $N$ -th harmonic generated by a mode of helical index  $m_L$  leads to an electric field  $\mathbf{E} \sim e^{i(Nm_L \pm (N-1)\Phi)}$ ; the supplemental term  $Nm_L\Phi$  in the phase is a pure interference effect. Our numerical results are similar to those observed by Hensing et al [1]. To our knowledge this study is

\* madalina.boca@unibuc.ro

the first to consider the coherent Thomson scattering of structured light on an ensemble of electrons; our results could be also of importance for various applications of the interaction of helical light with matter [23–25].

The analytical formulas are written in the international system of units, and for the numerical results we adopted the atomic system of units.

*The local plane wave approximation.* We consider the coherent scattering of a Laguerre - Gauss mode of the monochromatic electromagnetic field of frequency  $\omega_L$  on a system of electrons initially at rest, distributed uniformly in a disk of radius  $\varrho_m$ , equal to at least the beam radius, placed in the focal plane of the laser. The electromagnetic field propagating along the  $Oz$  direction of the reference frame can be written in the paraxial approximation in terms of an approximate solution of the Helmholtz equation, named Laguerre Gauss solution  $u_{p_L m_L}(\mathbf{r})$ ; its expression in cylindrical coordinates  $(\varrho_0, \Phi_0, z)$  is  $u_{p_L m_L}(\mathbf{r}) = v_{p_L m_L}(\varrho_0, z) e^{im_L \Phi_0}$  the product between a function  $v$  dependent on  $\varrho_0$  and  $z$  and the exponential  $e^{im_L \Phi_0}$ . The detailed expressions of  $v_{p_L m_L}$  and of the electromagnetic field are discussed in the supplemental material [26], Sect. I. A. We shall study the scattering of a monochromatic LG beam (assumed to be adiabatically introduced in the distant past) on a statistical ensemble of electrons, initially at rest, positioned in the focal plane of the laser. The laser wavelength that we consider is  $\lambda = 800$  nm, corresponding to  $\omega_L = 0.057$  au, and the beam waist  $w_0$  will be taken  $w_0 = 75\lambda$ , well within the validity of the paraxial approximation (see e.g. [27], Cap. 7). For this choice the variation of the field in the transversal plane is very slow and it can be considered as constant along distances of the order of the wavelength  $\lambda$  in the  $Oxy$  plane.

The motion of an electron in a plane wave monochromatic field of wavelength  $\lambda$ , and dimensionless intensity parameter  $\xi_0 = \frac{|e_0|E_0}{\omega m_e c}$  consists in an oscillation in the polarization plane, of amplitude  $r_\perp \sim \frac{c\xi_0}{\omega_L} \sim \xi_0 \lambda$ , and a displacement along the propagation direction  $z \sim \frac{c\xi_0^2}{2\omega_L} \sim \xi_0^2 \lambda$ . From this estimation it follows that an electron interacting with a structured field, such as a helical beam, will see only a monochromatic plane wave field whose amplitude depends on its initial position in the focal plane if the variation of the field intensity in the focal plane is slow and the intensity  $\xi_0 \lesssim 1$ . For the case of a helical beam, this condition is satisfied if the beam waist parameter  $w_0$  is large with respect to  $\lambda$ ; in our work, we consider  $w_0 = 75\lambda$ .

Then, if the initial cylindrical coordinates of the electron in the focal plane are  $\Phi_0, \varrho_0$  the electromagnetic field felt by the electron can be approximated as

$$\begin{aligned} \tilde{\mathbf{E}}(\mathbf{r}, t) &= \mathcal{E}_0(\varrho_0) \Re \left\{ \mathbf{e} e^{-i(\omega_L t - k z - m_L \Phi_0)} \right\}, \\ \tilde{\mathbf{B}}(\mathbf{r}, t) &= \frac{1}{c} \mathbf{e}_z \times \tilde{\mathbf{E}}(\mathbf{r}, t), \end{aligned} \quad (1)$$

where  $\mathcal{E}_0(\varrho_0)$  is the local amplitude of the field  $\mathcal{E}_0(\varrho_0) =$

$E_0 v_{p_L m_L}(\varrho_0, z = 0)$  and  $\mathbf{e}$  is the polarization vector, chosen as  $\mathbf{e} = e_x \zeta_x + i e_y \zeta_y$ . We can define a local intensity parameter  $\xi(\varrho_0) = \xi_0 v(\varrho_0, z = 0)$ ; in our model each electron feels a plane wave monochromatic field whose magnitude  $\mathcal{E}_0$  and initial phase  $m_L \Phi_0$  are remnants of the incident field structure. We name this approach the local plane wave approximation (LPWA) and we can test its validity by comparing the solution of the exact equations of motion with those for a particle in the external field (1). A detailed analysis presented in the supplemental material [26] shows that for  $\xi_0 \lesssim 1$  and  $w_0 \geq 70\lambda$ , LPWA can be used instead of the exact treatment.

*Coherent Thomson scattering in LPWA.* The problem of the non-linear Thomson scattering of a monochromatic plane wave on a charged particle is well studied in the literature [6, 28]; we review here briefly the main results.

We will consider an electron of charge  $e_0$  having the initial position  $\mathbf{r}(t_{in}) = \mathfrak{R}_0$  in the focal plane  $Oxy$ , of cylindrical coordinates  $\mathfrak{R}_0 \equiv (\varrho_0, \Phi_0, z = 0)$ , moving along the trajectory  $\mathbf{r}(t)$  in the field (1). We define the electron trajectory relative to the initial position of the particle  $\mathfrak{R}_0$ ,  $\mathbf{r}_0(t) = \mathbf{r}(t) - \mathfrak{R}_0$ , and the relative observation point  $\mathbf{x}_0 = \mathbf{x} - \mathfrak{R}_0$ , whose unity vector is  $\mathbf{n}_0 = \frac{\mathbf{x}_0}{|\mathbf{x}_0|}$  of polar angles  $\theta_0, \phi_0$ .

In the LPWA the electron is at the initial moment in the plane  $Oxy$ , having the cylindrical coordinates  $(\varrho = \varrho_0, \varphi = \Phi_0, z = 0)$  and moves under the influence of a local plane wave field (1), of intensity dependent on the radial coordinate  $\xi(\varrho_0)$ , and initial phase dependent on the initial azimuthal coordinate  $\Phi_0$  of the electron. Using the analytical expression of the trajectory and of the velocity of the particle we obtain, after a straightforward calculation [6] the Fourier transform of the emitted fields. The frequency spectrum of the emitted radiation is discrete, consisting of equidistant lines

$$\omega_N = N \frac{\omega_L}{\alpha}, \quad \alpha = 1 + \frac{\xi^2(\varrho_0)}{4} (1 - \cos \theta_0) \quad (2)$$

the Fourier transform of the field being expressed as an infinite series of the form

$$\begin{aligned} \mathbf{E}(\mathbf{x}, \omega; \varrho_0, \Phi_0) &= \sum_{N=-\infty}^{\infty} \tilde{\mathbf{E}}_N(\mathbf{x}; \varrho_0, \Phi_0) \delta(\omega - \omega_N) \\ \mathbf{B}(\mathbf{x}, \omega; \varrho_0, \Phi_0) &= \mathbf{n}_0 \times \mathbf{E}(\mathbf{x}, \omega; \varrho_0, \Phi_0) \end{aligned} \quad (3)$$

where the coefficients  $\tilde{\mathbf{E}}_N$  can be written in terms of generalized Bessel functions; for the details of calculation and their explicit form see the supplemental material [26], Sect. II. C; in the previous equation we indicated explicitly the dependence on the initial coordinates of the electron  $\varrho_0, \Phi_0$ . The calculation is done in the long distance approximation, which requires  $|\mathbf{x}_0| \gg |\mathbf{r}_0|$ , with no restriction on  $\mathfrak{R}_0$ . We can easily check that  $\tilde{\mathbf{E}}_{-N}(\mathbf{x}) = (\tilde{\mathbf{E}}_N(\mathbf{x}))^*$  as it should be, since the electric field is real  $\mathbf{E}(\mathbf{x}, t) \in \mathbb{R}^3$ , so in the following we can consider only the positive values of the harmonic index,  $N \geq 1$ .

In the second part of our calculation, we consider the coherent emission of radiation by a collection of electrons distributed in the focal plane of the laser; this distribution is modelled as a continuous thin electron sheet, characterized by the uniform surface charge density  $\sigma_0$ ; for simplicity, in the numerical calculation, we choose  $\sigma_0 = 1$  au. Summation over the electrons will be then replaced by integration over all the values of  $\mathfrak{R}_0 \in Oxy$  plane. We will present results for the field measured on a screen, orthogonal to the laser propagation direction, at a large distance  $z = Z \gg w_0$  from the focal plane.

The temporal Fourier transform of the total field measured in a point  $\mathbf{x} = (x, y, Z)$  on the screen will be

$$\begin{aligned} \mathbf{E}_{tot}(\mathbf{x}, \omega) &= \sum_{N=-\infty}^{\infty} \int_{\mathfrak{R}_0} d^2 a \tilde{\mathbf{E}}_N(\mathbf{x}; \varrho_0, \Phi_0) \delta(\omega - \omega_N) \\ &\equiv \sum_{N=-\infty}^{\infty} \tilde{\mathbf{E}}_{N,tot}(\mathbf{x}, \omega) \end{aligned} \quad (4)$$

In the previous equation  $\omega_N$ , defined in (2) depends on the integration variable  $\mathfrak{R}_0$  through  $\theta_0$  and the argument  $\varrho_0$  of  $\xi$ . However, due to the interference effects, at large  $Z$  the radiation is confined inside of a cone of opening angle of the order of magnitude  $\sim \frac{\lambda}{w_0}$  which means that scattering angles appearing in the frequency formula are very small  $\theta_0 \sim 10^{-2}$ . Taking into account also the fact the  $\xi(\varrho_0) \leq 1$  we can see that when the integration variable  $\mathfrak{R}_0$  changes in the focal plane of the laser, the values of  $\omega_N$  corresponding to a fixed  $N$  have only very small variations

$$\omega_N(\varrho_0, \Phi_0) = N\omega_L(1 + \varepsilon(\varrho_0, \Phi_0)), \quad \varepsilon(\varrho_0, \Phi_0) \ll 1. \quad (5)$$

Then we define the  $N$ th Fourier component of the total field as an integral over a small interval  $\Delta\omega \ll \omega_L$

$$\begin{aligned} \mathbf{E}_{N,tot}(\mathbf{x}) &\equiv \int_{N\omega_L - \Delta/2}^{N\omega_L + \Delta/2} d\omega \tilde{\mathbf{E}}_{N,tot}(\mathbf{x}, \omega) \\ &= \int_0^{\varrho_m} d\varrho_0 \varrho_0 \int_0^{2\pi} d\Phi_0 \tilde{\mathbf{E}}_N(\mathbf{x}; \varrho_0, \Phi_0) \\ \mathbf{B}_{N,tot}(\mathbf{x}) &\equiv \frac{1}{c} \int_0^{\varrho_m} d\varrho_0 \varrho_0 \int_0^{2\pi} d\Phi_0 (\mathbf{n}_0 \times \tilde{\mathbf{E}}_N(\mathbf{x}; \varrho_0, \Phi_0)) \end{aligned} \quad (6)$$

If the incident field is circularly polarized  $\zeta_x = \pm\zeta_y$  the calculation presented in detail in [26], Sect. II. C shows that the field recorded in a point of cylindrical coordinated  $\varrho, \Phi$  on the screen at the distance  $Z \gg w_0$  from the focal spot can be written as

$$\tilde{\mathbf{E}}_{N,tot}(\mathbf{x}) = e^{i(m_L N + \epsilon_L(N-1))\Phi} \int_0^{\varrho_m} d\varrho_0 \varrho_0 \mathbf{h}(\varrho, Z; \varrho_0) \quad (7)$$

where  $\epsilon_L$  is the handedness of the circular polarization  $\epsilon_L = \frac{\zeta_x}{\zeta_y} = \pm 1$ ; one can see that the field has a spatial structure of helical shape with a phase index

$$q = m_L N + \epsilon_L(N - 1) \quad (8)$$

dependent on the harmonic index and on the helical index of the incident beam. This structure should be observable experimentally, since the frequency of each harmonic is distinct.

*Results and discussion.* In this section we present numerical results for the scattered field for different parameters of the laser beam, in all cases we shall take the dimensionless intensity parameter  $\xi_0 = 0.1$ , the beam waist parameter  $w_0 = 75\lambda$ , the laser wavelength  $\lambda = 800$  nm, which corresponds to a frequency  $\omega_L = 0.057$  au and the helicity  $\epsilon_L = 1$ .

We start by analyzing the Poynting vector of the emitted radiation. In Fig 1 we presented the component  $S_z$

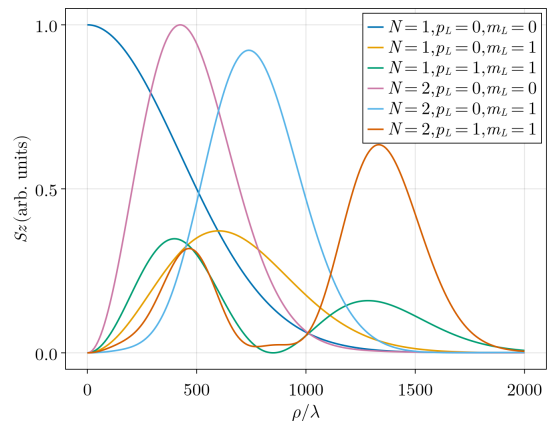


FIG. 1. The  $Oz$  component of the Poynting vector  $\mathbf{S}$  measured in the plane  $Z = 2 \times 10^5 \lambda$  ( $\sim 16$ cm) for  $N = 1, 2$ , and for different mode indices  $p_L, m_L$  (as written in the legend). For each  $N$ , the values of  $S_z$  were scaled by the factor  $s = \max(S_z)(p_L = m_L = 0)$  (the maximum of  $S_z$  for the same  $N$  and  $p_L = m_L = 0$ ). The scaling factors are  $s = 0.1$  au ( $N = 1$ ), and  $s = 1.7 \times 10^{-9}$  au ( $N = 2$ ).

measured on a screen at the distance  $Z = 2 \times 10^5 \lambda$  from the focal plane, for three combinations of values for the indices  $p_L, m_L$ : (0, 0), (0, 1), and (1, 1), for the first and the second harmonic. In all cases the the shape of  $S_z$  distribution has cylindrical symmetry in the screen plane, so it is enough to represent it as a function of the cylindrical coordinate  $\varrho$ . As the distance  $Z$  is much larger than the laser wavelength, due to the interference effects between the electromagnetic field emitted from different points in the focal plane, the radiation is emitted into a cone of very small opening angle (similar to the Fraunhofer diffraction). The opening angle can be estimated from the ratio of the radial extension of the distribution measured on the screen to the value of  $Z$ . We obtain in all cases  $\Theta_0 \sim \frac{1}{100}$ , in agreement with the ratio of the laser wavelength to the beam diameter. The interference

pattern consists of concentric rings whose position and size depend on  $N, p_L, m_L$ ; the only case when a central maximum is present is for the fundamental harmonic and  $p_L = m_L = 0$ .

We can see very large differences between the numerical values of the fundamental and the second harmonic (see the values of the scaling factors  $s$  defined in the figure caption); they are due to two factors: one the one hand, the electric field depends on the "local scattering angle"  $\theta_0$  as  $\mathbf{E}_n \sim \theta_0^{N-1}$  and as the scattering takes place mostly in the forward direction,  $\theta_0$  will be of the order of  $\Theta_0 \approx 10^{-2}$ . On the other hand, the emitted field  $E_N$  depends also on the dimensionless parameter  $\xi_0$  as  $E_N \sim \xi_0^N$  which introduces an additional factor of  $10^2$  between  $S_z(N=1)$  and  $S_z(N=2)$ .

Besides the cylindrical symmetry, the Poynting vector obeys also a scaling law with respect to  $\varrho$  and  $Z$ . We have checked that for  $Z \geq 10^5 \lambda$  the relation

$$Z^2 S_z(\varrho, Z) = \text{fct}\left(\frac{\varrho}{Z}\right) \quad (9)$$

is obeyed with very good accuracy, which means that at large distance from the focal plane the shape of the energy distribution of the emitted radiation propagates undistorted inside a cone of given opening angle.

However, as we will see next, the electric and magnetic components of the field have more complex properties. The following two figures present the electric field and its phase, for the fundamental Gaussian mode of the incident field ( $p_L = m_L = 0$ ) and for a Laguerre - Gauss incident beam ( $m_L \neq 0$ ).

In Fig. 2 we present the  $Ox$  component of the emitted electric field for  $p_L = m_L = 0$ ,  $N = 1$  (a, d) and  $N = 2$  (c, f) and for  $p_L = m_L = 1$ ,  $N = 1$  (b, e). In all cases the distance  $Z$  is  $2 \times 10^5 \lambda$ . The upper row shows the real part of  $E_x$ , and the lower row, its phase. For  $N = 1$  the emitted field is essentially identical to the incident one: for  $m_L = 0$  there is no azimuthal dependence of the electric field and for  $m = 1$ , it has a helical structure  $E_x \sim e^{i\Phi}$ . A similar azimuthal structure of the emitted field is formed also for  $m_L = 0$   $N = 2$  (b and e). In all cases the dependence of  $\Phi$  is in agreement with Eq. (7); we thus obtained the same shape of the helical wavefront in two different scenarios: the fundamental of the helical mode  $m_L = 1$ , or the second harmonic of the fundamental Gaussian mode. It is also in good agreement with the experimental result presented by Hemsing *et al* [1]; in their work, the field was obtained by scattering of a Gaussian mode on a helically modulated electron beam, while in our case the modulation is done by the incident field itself.

The radial dependence of the electric field is different in the three cases, (see also the energy distribution for the same parameters in the previous figure) and the numerical values are much lower for the second harmonic than the fundamental.

The results are similar for the case  $N = 2$ ,  $p_L = 2$ ,

$m_L = \pm 2$  presented in Fig. 3 showing the real part of the component  $E_x$  of the electric field (panels (a) and (d)) and the phase of the  $E_x$  (panels (b) and (e)), at the same distance  $Z = 2 \times 10^5 \lambda$ . The Poynting vector has a structure of concentric rings similar to those in Fig. 1 and is not represented. In the graphics of the phase of  $E_x$  there are two distinct regions: an inner region of radius  $\varrho_1 \sim 400 \lambda$  in which the phase changes slowly with  $\varrho$ , and the outer region in which the phase changes very fast with  $\varrho$ , giving rise to a spiral-like figure, in agreement with the behavior predicted in the supplemental material [26], and with the experimental observation presented in [1]. Panels (c) and (f) contain graphics of the phase of  $E_x$  as a function of the angle  $\Phi$  in the observation plane for three values of  $\varrho$ , chosen to correspond to the radii of the concentric rings in which the radiation is emitted  $\varrho = 530 \lambda$ ,  $1150 \lambda$  and  $1910 \lambda$ . In all cases we can see the very good agreement with the behavior predicted by Eq. (7); even in the outer region, where  $\arg(E_x)$  changes very fast with  $\varrho$ , for fixed  $\varrho$  the phase depends linearly on  $\Phi$ , with the coefficient

$$q = Nm_L + (N-1)\epsilon_L = \begin{cases} -3, & m_L = -2 \\ 5, & m_L = 2 \end{cases} \quad (10)$$

We have also checked that in all cases  $\arg E_x = \frac{\pi}{2} - \arg E_y$ , which confirms that the emitted radiation is circularly polarized.

*Conclusion.* In conclusion, we have demonstrated that the coherent scattering of a monochromatic field described by a Laguerre-Gauss mode by a 2D continuous electron distribution will generate structured helical light. Our approach is based on a local plane wave approximation whose validity is estimated theoretically and tested numerically (see the supplemental material [26]); the model is valid for incident fields having the dimensionless intensity parameter up to  $\xi_0 \lesssim 1$  and the beam waist  $w_0 \geq 75 \lambda$ . Our numerical calculations show that due to the interference effects the emitted field is concentrated into the forward direction, similar to the Fraunhofer diffraction, if the incident field is circularly polarized, each harmonic has a helical spatial structure, with a given helical index  $q$  defined in (7); we can expect it to carry angular momentum proportional to the new helical index

A further test of our results will be to calculate the angular momentum of the scattered radiation in order to check the correlation with the spatial structure of the electric field described in the present paper.

*Acknowledgments.* P.-V. Toma acknowledges the financial support from the Romanian Ministry of Education consisting in a doctoral scholarship received through the Doctoral School of Physics of the University of Bucharest. This paper was supported by Council for Doctoral Studies (C.S.U.D.), University of Bucharest. P.-V. Toma was also funded from the Romanian Ministry of Education and Research under the Romanian National Nucleus Program LAPLAS VI, contract no. 30N/2023.

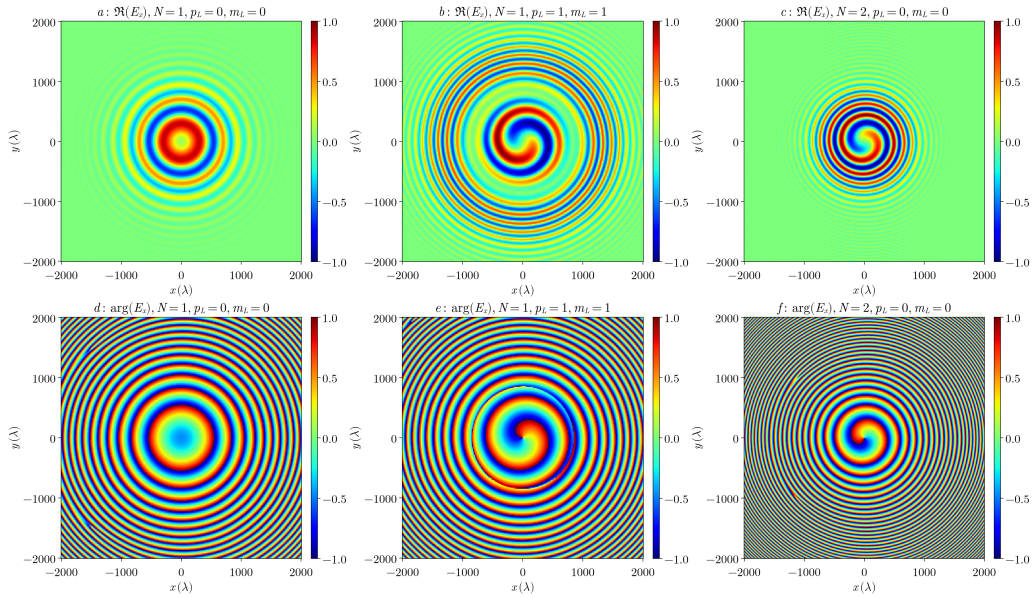


FIG. 2. The  $Ox$  component of the scattered field measured on a screen at  $Z = 2 \times 10^5 \lambda$ : the real part of the electric field scaled to  $(-1, 1)$  (the upper row), and its phase in units of  $\pi$  (the lower row). The laser field is circularly polarized with  $\epsilon_L = 1$  and  $\xi_0 = 0.1$ . (a)  $\Re(E_x)$  for  $N = 1$ ,  $p_L = m_L = 0$ , (scaling factor  $0.052$  au), (b)  $\Re(E_x)$  for  $N = 1$ ,  $p_L = m_L = 1$  (scaling factor  $s = 0.039$  au); (c)  $\Re(E_x)$  for  $N = 2$ ,  $m_L = p_L = 0$  (scaling factor  $s = 8.9 \times 10^{-6}$  au); (d), (e), (f) the phase of  $E_x$  in units of  $\pi$  for the same parameters as (a), respectively (b) and (c).

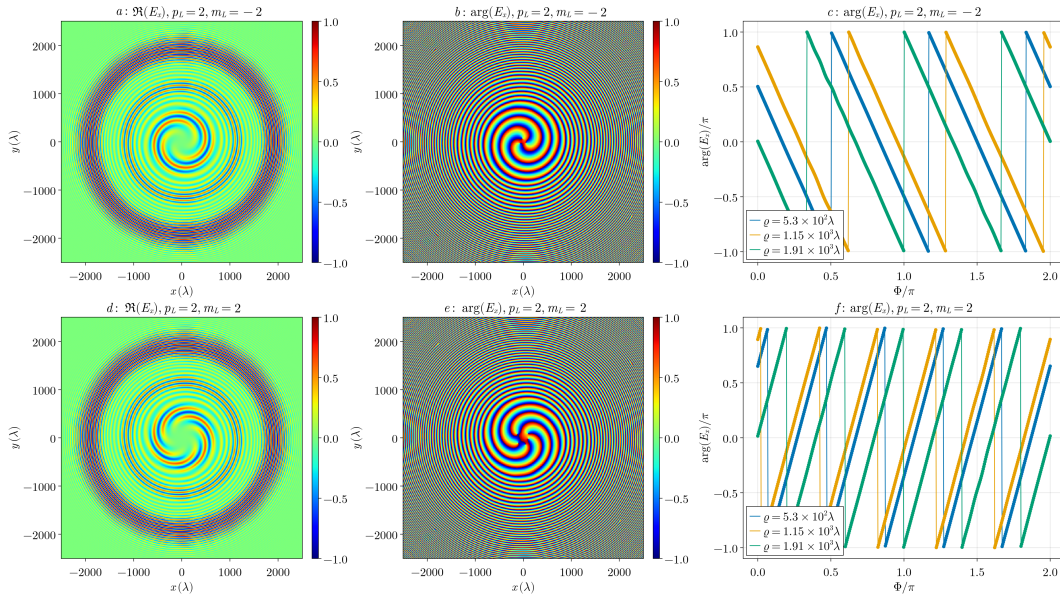


FIG. 3. The scattered field for  $Z = 2 \times 10^5 \lambda$ ,  $N = 2$ ,  $p_L = 2$ . (a), (d): the real part of  $E_x$  for  $m_L = 2$ , respectively  $m_L = -2$  (scaling factor  $1.0 \times 10^{-9}$  au), (b), (e): the phase of  $E_x$  in units of  $\pi$ , (c), (f): the phase of  $E_x$  as a function of the azimuthal angle  $\Phi$  in the observation plane for three fixed values  $\rho$  written in the legend, in units of  $\pi$ .

- 
- [1] E. Hemsing, A. Knyazik, M. Dunning, D. Xiang, A. Marinelli, C. Hast, and J. B. Rosenzweig, Coherent optical vortices from relativistic electron beams, *Nature Physics* **9**, 549 (2013).
- [2] T. Taira, Yoshitaka and Hayakawa and M. Katoh, Gamma-ray vortices from nonlinear inverse thomson scattering of circularly polarized light, *Scientific Reports* **7**, 5018 (2017).
- [3] E. S. Sarachik and G. T. Schappert, Classical theory of the scattering of intense laser radiation by free electrons, *Phys. Rev. D* **1**, 2738 (1970).
- [4] G. A. Krafft, Spectral distributions of thomson-scattered photons from high-intensity pulsed lasers, *Phys. Rev. Lett.* **92**, 204802 (2004).
- [5] S. K. Ride, E. Esarey, and M. Baine, Thomson scattering of intense lasers from electron beams at arbitrary interaction angles, *Phys. Rev. E* **52**, 5425 (1995).
- [6] Y. Salamin and F. Faisal, Harmonic generation by super-intense light scattering from relativistic electrons, *Phys. Rev. A* **54**, 4383 (1996).
- [7] Y. I. Salamin and F. H. M. Faisal, Harmonic generation by scattering circularly polarized light of arbitrary intensity from free electrons of arbitrary initial velocity, *Phys. Rev. A* **55**, 3964 (1997).
- [8] G. A. Krafft, Spectral distributions of thomson-scattered photons from high-intensity pulsed lasers, *Phys. Rev. Lett.* **92**, 204802 (2004).
- [9] G. A. Krafft, A. Doyuran, and J. B. Rosenzweig, Pulsed-laser nonlinear thomson scattering for general scattering geometries, *Phys. Rev. E* **72**, 056502 (2005).
- [10] F. Cajiao Vélez, J. Z. Kamiński, and K. Krajewska, Electron scattering processes in non-monochromatic and relativistically intense laser fields, *Atoms* **7**, 10.3390/atoms7010034 (2019).
- [11] V. Bordovitsyn, O. Konstantinova, and E. Nemchenko, Angular momentum of synchrotron radiation, *Russ Phys J* **55**, 44 (2012).
- [12] M. Katoh, M. Fujimoto, H. Kawaguchi, K. Tsuchiya, K. Ohmi, T. Kaneyasu, Y. Taira, M. Hosaka, A. Mochihashi, and Y. Takashima, Angular momentum of twisted radiation from an electron in spiral motion, *Phys. Rev. Lett.* **118**, 094801 (2017).
- [13] V. Epp and U. Guselnikova, Angular momentum of radiation from a charge in circular and spiral motion, *Physics Letters A* **383**, 2668 (2019).
- [14] V. Epp, U. Guselnikova, and I. Kamenskaya, Angular momentum transferred by the field of a moving point charge, *Phys. Rev. A* **105**, 023511 (2022).
- [15] Y. Lian, X. Qi, Y. Wang, Z. Bai, Y. Wang, and Z. Lu, Oam beam generation in space and its applications: A review, *Optics and Lasers in Engineering* **151**, 106923 (2022).
- [16] L. Pengfei, L. Peixiang, and C. Wei, Spatial characteristics of thomson scattering in a linearly polarized field, *Plasma Science and Technology* **9**, 143 (2007).
- [17] K. Li, L. Li, Q. Shu, Y. Tian, Y. Shi, and Z. Zhang, Spatial characteristics of motion and emission from electron driven by linearly polarized tightly focused laser pulses, *Optik* **183**, 813 (2019).
- [18] K. Liu, T. Yu, D. Zou, X. Xu, Y. Yin, and F. Shao, Twisted radiation from nonlinear thomson scattering with arbitrary incident angle, *The European Physical Journal D* **74**, 7 (2020).
- [19] Y. Wang, Q. Zhou, J. Zhuang, P. Yu, and Y. Tian, Vortex and symmetric radiation character of nonlinear thomson scattering in laguerre-gaussian circularly polarized laser pulses, *Opt. Express* **29**, 22636 (2021).
- [20] O. Vais and V. Bychenkov, Nonlinear thomson scattering of a tightly focused relativistically intense laser pulse by an ensemble of particles, *Quantum Electronics* **50**, 922 (2020).
- [21] I. Pastor, R. F. Álvarez Estrada, L. Roso, F. Castejón, and J. Guasp, Nonlinear relativistic electron thomson scattering for laser radiation with orbital angular momentum, *Journal of Physics Communications* **4**, 065010 (2020).
- [22] M. Mokrov, M. Shneider, and A. Gerakis, Analysis of coherent thomson scattering from a low temperature plasma, *Physics of Plasmas* **29**, 033507 (2022).
- [23] P.-V. Toma, S. Micluta-Câmpeanu, M. Boca, and V. Băran, Angular momentum transfer to charged particles by interaction with Laguerre-Gauss pulses, *AIP Advances* **14**, 065109 (2024), [https://pubs.aip.org/aip/adv/article-pdf/doi/10.1063/5.0205865/19980311/065109\\_1\\_5.0205865.pdf](https://pubs.aip.org/aip/adv/article-pdf/doi/10.1063/5.0205865/19980311/065109_1_5.0205865.pdf).
- [24] Z.-W. Lu, L. Guo, Z.-Z. Li, M. Ababekri, F.-Q. Chen, C. Fu, C. Lv, R. Xu, X. Kong, Y.-F. Niu, and J.-X. Li, Manipulation of giant multipole resonances via vortex  $\gamma$  photons, *Phys. Rev. Lett.* **131**, 202502 (2023).
- [25] Y. Xu, D. L. Balabanski, V. Baran, C. Iorga, and C. Matei, Vortex photon induced nuclear reaction: Mechanism, model, and application to the studies of giant resonance and astrophysical reaction rate, *Physics Letters B* **852**, 138622 (2024).
- [26] See Supplemental Material at URL-will-be-inserted-by-publisher.
- [27] A. Siegman, *Lasers* (University Science Books, 1986).
- [28] J. H. Eberly, Interaction of very intense light with free electrons (Elsevier, 1969) pp. 359–415.

# Supplemental material for "Coherent Thomson scattering of Laguerre - Gauss beams on an electron sheet"

Petru-Vlad Toma <sup>1,2</sup> Andrei Cristian Opinca,<sup>2</sup> Virgil Baran <sup>2,3</sup> and Madalina Boca <sup>2,\*</sup>

<sup>1</sup>*Center for Advanced Laser Technologies, National Institute for Laser,  
Plasma and Radiation Physics, Magurele, Romania*

<sup>2</sup>*University of Bucharest, Department of Physics, Magurele, Romania*

<sup>3</sup>*Academy of Romanian Scientists, Strada Ilfov 3, Sector 5, 050044, Bucharest, Romania*

(Dated: August 9, 2024)

## CONTENTS

10	I. The electromagnetic field and the local plane wave approximation	1
11	A. The Laguerre-Gauss modes of the electromagnetic field	1
12	B. The local plane wave approximation (LPWA)	2
13	II. Thomson scattering of Laguerre Gauss beams	8
14	A. Fourier analysis of the emitted fields - large distance approximation	8
15	B. The trajectory of a particle in a monochromatic field	9
16	C. The field emitted by a particle in an LG beam	10
17	1. The case of circular polarization	13
18	III. Integration over the initial electron distribution	13
19	A. Analytical estimation of the phase of the emitted field in the circular polarization case	14
20	References	15

## I. THE ELECTROMAGNETIC FIELD AND THE LOCAL PLANE WAVE APPROXIMATION

### A. The Laguerre-Gauss modes of the electromagnetic field

In the present work we consider the coherent scattering of a Laguerre - Gauss mode of the monochromatic electromagnetic field of frequency  $\omega_L$  on a system of electrons initially at rest, distributed uniformly in a disk of radius  $\varrho_m$ , at least equal to the beam radius, placed in the focal plane of the laser. The incident electric field of the beam propagating along the  $Oz$  direction of the reference frame can be written in the paraxial approximation as [1]

$$\begin{aligned}
 E_x(\mathbf{r}, t) &= E_0 \Re \{ \zeta_x u_{p_L m_L}(\mathbf{r}) f(\varphi) \}, & E_y(\mathbf{r}, t) &= E_0 \Re \{ i \zeta_y u_{p_L m_L}(\mathbf{r}) f(\varphi) \}, & f(\varphi) &= e^{-i\varphi}, & \varphi &= \omega_L t - k_L z \\
 E_z(\mathbf{r}, t) &= E_0 \Re \left\{ -\frac{1}{ik} \left[ \zeta_x \frac{\partial u_{p_L m_L}(\mathbf{r})}{\partial x} + i \zeta_y \frac{\partial u_{p_L m_L}(\mathbf{r})}{\partial y} \right] f(\varphi) \right\}
 \end{aligned} \tag{1}$$

In the expressions above the components in the plane orthogonal on the propagation direction,  $E_{x,y}$  are written in terms of the Laguerre-Gauss solution of the Helmholtz equation in the paraxial approximation,  $u_{p_L m_L}(\mathbf{r}) e^{ik_L z}$  with  $k_L = \frac{\omega_L}{c}$ , the polarization being fixed by the two real constants  $\zeta_x, \zeta_y$  chosen such that  $\zeta_x^2 + \zeta_y^2 = 1$ ; for example,  $\zeta_x = \pm \zeta_y = \frac{1}{\sqrt{2}}$  corresponds to circular polarization and  $\zeta_x = 1, \zeta_y = 0$  describe the linear polarization along  $Ox$ . The amplitude of the electric field is conveniently expressed in terms of a dimensionless parameter  $\xi_0$

$$E_0 = \frac{\omega_L m_e c \xi_0}{|e_0|} \tag{2}$$

---

\* madalina.boca@unibuc.ro

with  $m_e$  and  $e_0$  the electron mass and charge, and  $c$  the velocity of light in vacuum. The component of  $\mathbf{E}$  along the propagation direction,  $E_z$  is calculated from the condition that  $\nabla \cdot \mathbf{E} = 0$ , using, in the paraxial approximation  $\partial_z E_z \approx ik_L E_z$ . Similarly, the magnetic field is calculated from the Maxwell equations

$$\partial_t \mathbf{B} = -\nabla \times \mathbf{E}, \quad \nabla \cdot \mathbf{B} = 0, \quad (3)$$

using  $\partial_t \mathbf{B} = -i\omega_L \mathbf{B}$  and again the paraxial approximation, with the result

$$\begin{aligned} B_x(\mathbf{r}, t) &= \frac{E_0}{c} \Re \{-i\zeta_y u_{p_L m_L}(\mathbf{r}) f(\varphi)\}, & B_y(\mathbf{r}, t) &= \frac{E_0}{c} \Re \{\zeta_x u_{p_L m_L}(\mathbf{r}) f(\varphi)\} \\ B_z(\mathbf{r}, t) &= \frac{E_0}{c} \Re \left\{ -\frac{1}{ik} \left[ -i\zeta_y \frac{\partial u_{p_L m_L}(\mathbf{r})}{\partial x} + \zeta_x \frac{\partial u_{p_L m_L}(\mathbf{r})}{\partial y} \right] f(\varphi) \right\} \end{aligned} \quad (4)$$

The explicit expression of  $u_{p_L m_L}(\mathbf{r})$  is, in cylindrical coordinates  $\varrho_0, \Phi_0, z$ ,

$$\begin{aligned} u_{p_L m_L}(\varrho_0, \Phi_0, z) &\equiv v_{p_L m_L}(\varrho_0, z) e^{im_L \Phi_0} = \\ u_{p_L m_L}(\varrho_0, \Phi_0, z) &= N_{p_L |m_L|} \frac{w_0}{w(z)} \left( \frac{\sqrt{2}}{w(z)} \right)^{|m_L|} e^{-i(2p_L + |m_L| + 1)\psi_G(z)} e^{-\frac{k}{2} \frac{\varrho_0^2}{z_R + iz}} \\ &\quad \times {}_1F_1(-p_L, |m_L| + 1, \frac{2\varrho_0^2}{w(z)^2}) \varrho_0^{|m_L|} e^{im_L \Phi_0}, \quad p_L \in \mathbb{N}, \quad m_L \in \mathbb{Z} \end{aligned} \quad (5)$$

where  $w(z) = w_0 \sqrt{1 + \frac{z^2}{z_R^2}}$ ,  $w_0$  being the beam waist,  $z_R$  is the Rayleigh radius,  $z_R = \frac{kw_0^2}{2}$ , and  $\psi_G$  the Gouy phase  $\Psi_g = \arctan \frac{z}{z_R}$ . The normalization constant is

$$N_{p_L m_L} = \frac{\sqrt{2}}{|m_L|!} \sqrt{\frac{(p_L + |m_L|)!}{p_L!}} \quad (6)$$

chosen such that the "nominal intensity" of the beam  $\mathcal{I}_0$  (the total power  $\mathcal{P}$  of the beam divided by  $\pi w_0^2$ ) to be  $\mathcal{I}_0 = \frac{\epsilon_0 c E_0^2}{2}$  [2].

In Fig 1 below we present the component  $E_x$  of the field, in the focal plane of the laser ( $z = 0$ ), at the moments  $t = 0$ ,  $t = T/4$ ,  $t = T/2$ , and  $t = 3T/4$ ,  $T$  being the period of the field  $T = 2\pi/\omega_L$ . The parameters of the LG mode are  $p_L = m_L = 2$ , and the polarization is circular  $\zeta_x = \zeta_y = \frac{1}{\sqrt{2}}$ . The magnitude of the field, here in arbitrary units, is represented by color, according to the color scale next to each graph, and the units on the  $x, y$  axes are  $w_0$ . We can see the apparent "rotation" of the spatial structure due to the combination of the spatial and temporal phase of the field

$$\mathbf{E} \sim e^{im_L \Phi_0 - i\omega_L t}, \quad \Phi_0 = \arctan(y/x). \quad (7)$$

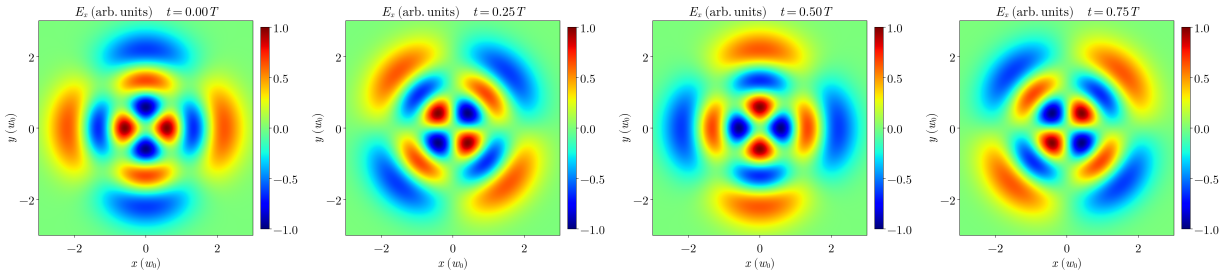


FIG. 1. The  $E_x$  component of the electromagnetic field represented in the focal plane  $z = 0$  at  $t = 0$ ,  $t = 0.25T$ ,  $t = 0.5T$ ,  $t = 0.75T$ .

47

## B. The local plane wave approximation (LPWA)

We shall study the scattering of a monochromatic LG beam (assumed to be adiabatically coupled in the very distant past) on a statistical ensemble of electrons, initially at rest, positioned in the focal plane of the laser. The

49

50 laser wavelength that we will consider is  $\lambda = 800$  nm, corresponding to  $\omega_L = 0.057$  au and the beam waist  $w_0$  will be  
 51 taken  $w_0 = 75\lambda$ , well within the validity of the paraxial approximation (see e.g. [3], Cap. 7). We notice that for this  
 52 choice the variation of the field in the transversal plane is very slow and the field can be considered as constant along  
 53 distances of the order of the wavelength  $\lambda$  in the  $Oxy$  plane.

54 We will show here that for beam waists much larger than  $\lambda$  and for the dimensionless intensity parameter  $\xi_0 \lesssim 1$   
 55 we can use an approximation based on the assumption that each electron, interacting with the laser beam feels the  
 56 electromagnetic field as a plane wave of amplitude and initial phase determined by the electron initial position.

57 Considering the expression of the trajectory of a charged particle of mass  $m_e$  and electric charge  $e_0$ , initially at rest  
 58 in a plane wave field, described in the Coulomb gauge by the vector potential  $\mathbf{A}(\phi)$  (see, for example [4], Eq. (A1))

$$z(t) = \frac{c}{2\omega_L} \int_{\varphi_0}^{\varphi} d\chi \frac{e_0^2 \mathbf{A}^2(\chi)}{(m_e c)^2}, \quad \mathbf{r}_\perp(t) = \frac{c}{\omega_L} \int_{\varphi_0}^{\varphi} d\chi \frac{e_0 \mathbf{A}(\chi)}{m_e c}, \quad \varphi = \omega_L t - kz. \quad (8)$$

59 it follows that the amplitude of the motion of the electron in a monochromatic field is of the order of magnitude of

$$r_\perp \sim \frac{c\xi_0}{\omega_L} \sim \xi_0 \lambda, \quad z \sim \frac{c\xi_0^2}{2\omega_L} \sim \xi_0^2 \lambda \quad (9)$$

60 where  $\xi_0$  is the dimensionless intensity parameter defined in Eq. (2). The analytical expression of the electron  
 61 momentum is

$$\begin{aligned} \mathbf{p}_\perp(\phi) &= -e \left( \mathbf{A}(\phi) - \mathbf{A}_0 + \frac{\mathbf{p}_{0\perp}}{e} \right), \\ p_z(\phi) &= \frac{e^2 \mathcal{A}^2(\phi)}{2(p_0^0 - p_0^3)} + p_{0z}, \quad \mathcal{A}^2(\phi) = (\mathbf{A}(\phi) - \mathbf{A}_0)^2 - \frac{2\mathbf{p}_{0\perp}}{e} \cdot (\mathbf{A}(\phi) - \mathbf{A}_0), \end{aligned} \quad (10)$$

62 with  $\mathbf{p}_0$  and  $\mathbf{A}_0$  the initial values of the momentum and, respectively, vector potential.

63 From the estimation (9) it follows that an electron in a helical beam of waist  $w_0 \gg \lambda$  and  $\xi_0 \lesssim 1$  will see only a  
 64 monochromatic plane wave field of amplitude given by its initial position in the focal plane; if the initial cylindrical  
 65 coordinates of the electron in the focal plane are  $\Phi_0, \varrho_0$  then the electromagnetic field felt by the electron can be  
 66 approximated as

$$\tilde{\mathbf{E}}(\mathbf{r}, t) = \mathcal{E}_0(\varrho_0) \Re \left\{ (\mathbf{e}_x \zeta_x + i \mathbf{e}_y \zeta_y) e^{-i(\omega_L t - kz - m_L \Phi_0)} \right\}, \quad \tilde{\mathbf{B}}(\mathbf{r}, t) = \frac{1}{c} \mathbf{e}_z \times \tilde{\mathbf{E}}(\mathbf{r}, t) \quad (11)$$

67 and

$$\mathcal{E}_0(\varrho_0) = \frac{m_e c \omega_L \xi(\varrho_0)}{|e_0|}, \quad \xi(\varrho_0) = \xi_0 N_{p_L m_L} \left( \frac{\sqrt{2} \varrho_0}{w_0} \right)^{|m_L|} e^{-\frac{\varrho_0^2}{w_0^2}} {}_1F_1(-p_L, |m_L| + 1, \frac{2\varrho_0^2}{w_0^2}) \quad (12)$$

68 i.e. each electron feels a plane wave monochromatic field whose magnitude  $\mathcal{E}_0$  and initial phase  $m_L \Phi_0$  are remnants  
 69 of the initial field structure. The function  $\xi(\varrho_0)$  defined in Eq. (12) is a local, position dependent intensity parameter  
 70 of the plane waves. We shall use the name *local plane wave approximation (LPWA)* for this approach and in the  
 71 following we shall discuss its validity.

72 We have integrated numerically the relativistic equations of motion for an electron in the presence of the electro-  
 73 magnetic field described exactly and in LPWA and we have compared the corresponding trajectories and momenta. In  
 74 both cases (exact and LPWA) the particle-field coupling was introduced using a smooth envelope of Gaussian shape

$$(\mathbf{E}, \mathbf{B}) \rightarrow (f(\varphi) \mathbf{E}, f(\varphi) \mathbf{B}), \quad f(\varphi) = \begin{cases} e^{-\frac{\varphi^2}{\tau^2}}, & \varphi < 0 \\ 1, & \varphi > 0 \end{cases} \quad \text{with } \tau = 10\pi. \quad (13)$$

75 and the electron was initially at rest in the plane  $z = 0$ ; the parameters of the field were  $\xi_0 = 1$ ,  $w_0 = 75\lambda$ ,  $p_L = 2$ ,  
 76  $m_L = 2$ , circular polarization. We present results for time  $t \in (0, 10T)$  (after the onset of the stationary regime). In  
 77 the left panel of Fig. 2 below we present the comparison for the variation in time of the component along the  $Ox$   
 78 axis,  $p_x$ , of a particle with the initial position  $(x_0, y_0) = (70\lambda, -32\lambda)$ , which shows differences of about 10% between  
 79 the exact and the approximated results. However, the accuracy of the approximation depends strongly on the initial  
 80 position of the particle. For example, for a particle initially at  $(x_0, y_0) = (160\lambda, -90\lambda)$ , the exact and the approximate  
 81 results are practically indistinguishable, as one can see in the right panel of Fig 2.

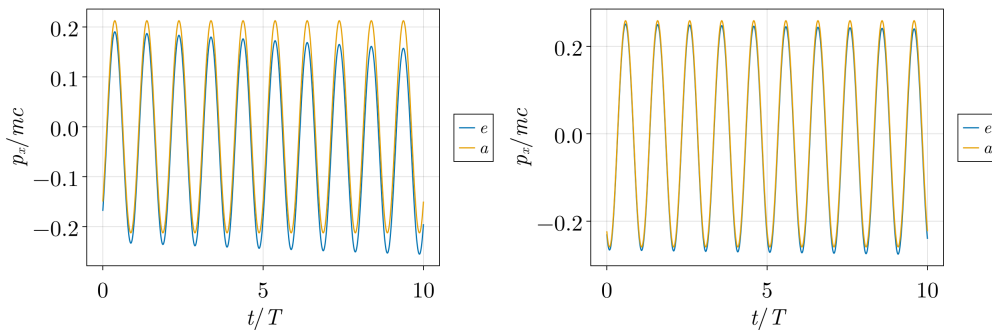


FIG. 2. Comparison between the exact results and the LPWA for the  $Ox$  component of the momentum of an electron interacting with a LG laser beam having  $\xi_0 = 1$ ,  $p_L = 2$ ,  $m_L = 2$ ,  $w_0 = 75\lambda$ ,  $\omega_L = 0,057$  au. Left: the initial position of the electron on the  $z = 0$  plane is  $(x_0, y_0) = (70\lambda, -32\lambda)$ ; right:  $(x_0, y_0) = (160\lambda, -90\lambda)$

82 Since the validity of the approximation depends strongly on the initial position of the particle in the focal plane,  
 83 we considered next a statistical ensemble of 10000 particles distributed randomly inside a disk of radius  $R_0 = 3.5w_0$   
 84 in the focal plane of the laser and we compared the exact and approximate results for each particle. We used the  
 85 same parameters as before,  $p_L = m_L = 2$ ,  $w_0 = 75\lambda$ ,  $\omega_L = 0.057$  a.u. and we consider two values of the dimensionless  
 86 intensity parameter  $\xi_0 = 0.5$  and  $\xi_0 = 1$ .

87 We compare the time evolution of the electron momenta for the two calculations: the exact one one and within  
 88 LPWA. We represent the electrons as dots in the plane  $Oxy$ , each dot having the same coordinates as those of the  
 89 initial position of the corresponding particle. The numerical values of a cartesian component of the momenta are  
 90 represented by the color of the dot; such that the variation of the momentum of an electron is seen as the change in  
 91 the color of the dot in the  $Oxy$  plane.

92 In Fig 3 we show in the upper rows 8 snapshots of the time evolution of the component  $p_x$  for  $\xi_0 = 0.5$ , calculated  
 93 using the exact equations of motion; the times  $t$  are written on top of each graph. The values of  $p_x$  are scaled to the  
 94 interval  $(-1, 1)$ , as shown by the colorbar, and the scaling factor (which is in this case the maximum of  $|p_x|$  over the  
 95 entire electron collection) is written at every moment also in the title of the graphic. We can see the spatial structure,  
 96 which is due to the fact that the "initial phase" of each electron momentum is given by the particle initial position  
 97 in the plane, and also the spatial structure has an apparent rotation motion, due to the fact that the value of  $p_x$   
 98 for each electron oscillates in time, as can be seen, e.g. in Eq. (10). The first 4 snapshots are taken for  $t \in (0, T)$   
 99 and the last four are for  $t \in (9T, 10T)$ . Below each graphic with the distribution of  $p_x$  we represent a second graphic  
 100 which contains in the same representation the difference  $\delta p_x = p_x^{\text{exact}} - p_x^{\text{LPWA}}$ . As before the values are scaled to the  
 101 interval  $(-1, 1)$  and the scaling factor and the time is indicated on top of each graphic. The ratio of the maximum  
 102 of  $|\delta p_x|$  to the maximum of  $|p_x|$  (the ratio of the two scaling factors) is an indication of the accuracy of the LPWA  
 103 approximation.

104 We can see that for each particle  $Ox$  component of the momentum oscillates with the frequency  $\omega_L$  of the laser,  
 105 and the amplitude is essentially constant, dependent only on the initial position of the electron in the plane. By  
 106 comparing the maximum values written in the title of each figure we can see that the error is at most 4% at  $t = 0$   
 107 (this is the error accumulated during the turn-on of the field along the envelope  $f(\phi)$ ) and increases linearly in time  
 108 up to about 7.5% at  $t = 10T$ . The comparison of the  $Oy$  components of the momentum is not presented here since,  
 109 given the circular polarization of the field,  $p_x$  and  $p_y$  behave identically; in Fig. 4 we present the analysis of the  $Oz$   
 110 component of the momentum.

111 In this case the spatial distribution of  $p_z$  is almost constant; this property can be explained using the analytical  
 112 expression of the momentum in a plane wave field (10) with the initial condition  $p_0^3 = 0$ ,  $p_0^0 = mc$ ,  $\mathbf{A}_0 = 0$ . We can  
 113 see that if the field is circularly polarized  $p_z$  is constant, proportional to the square of the field amplitude, so the  
 114 concentric circles of different amplitudes in Fig. 4 are in fact a representation of the transversal intensity profile of  
 115 the beam. Also in this case, from the graphics of  $\delta p_z$  we see that the relative error changes between 6% at  $t = 0$   
 116 and 10% at  $t = 10T$ . Finally, by comparing the representations of  $p_x$  and  $p_z$  it follows that overall the longitudinal  
 117 component of  $\mathbf{p}$  is about 10% of the radial component.

118 Next, we have investigated the behavior with respect to  $\xi_0$ ; in Figs. 5, 6 we present the same comparison for  $\xi_0 = 1$

119 Firstly, we notice that the orthogonal component of  $\mathbf{p}$  increases proportional to  $\xi_0$ , and  $p_z$  depends quadratically  
 120 on  $\xi_0$ , as predicted by the analytical approximation (10). Also the overall errors are larger in this case: the relative  
 121 error of  $p_x$  changes from 8% to 16% in the time interval  $t \in (0, 10T)$  while for  $p_z$  the error changes from 12% to 25%.

122 We have checked that properties presented here for  $p_L = 2$ ,  $m_L = 2$  and circular polarization remain valid also for  
 123 different indices  $p$  and  $m$  and for elliptic or linear polarization; also the behavior with the waist  $w_0$  is that expected,  
 124 i.e. the accuracy of LPWA improves when  $w_0$  increases.

125 The conclusion of the present analysis is that LPWA is sufficiently accurate for intensities  $\xi_0 \lesssim 1$  and  $w_0 \geq 75$ , the  
 126 values used in our numerical simulations.

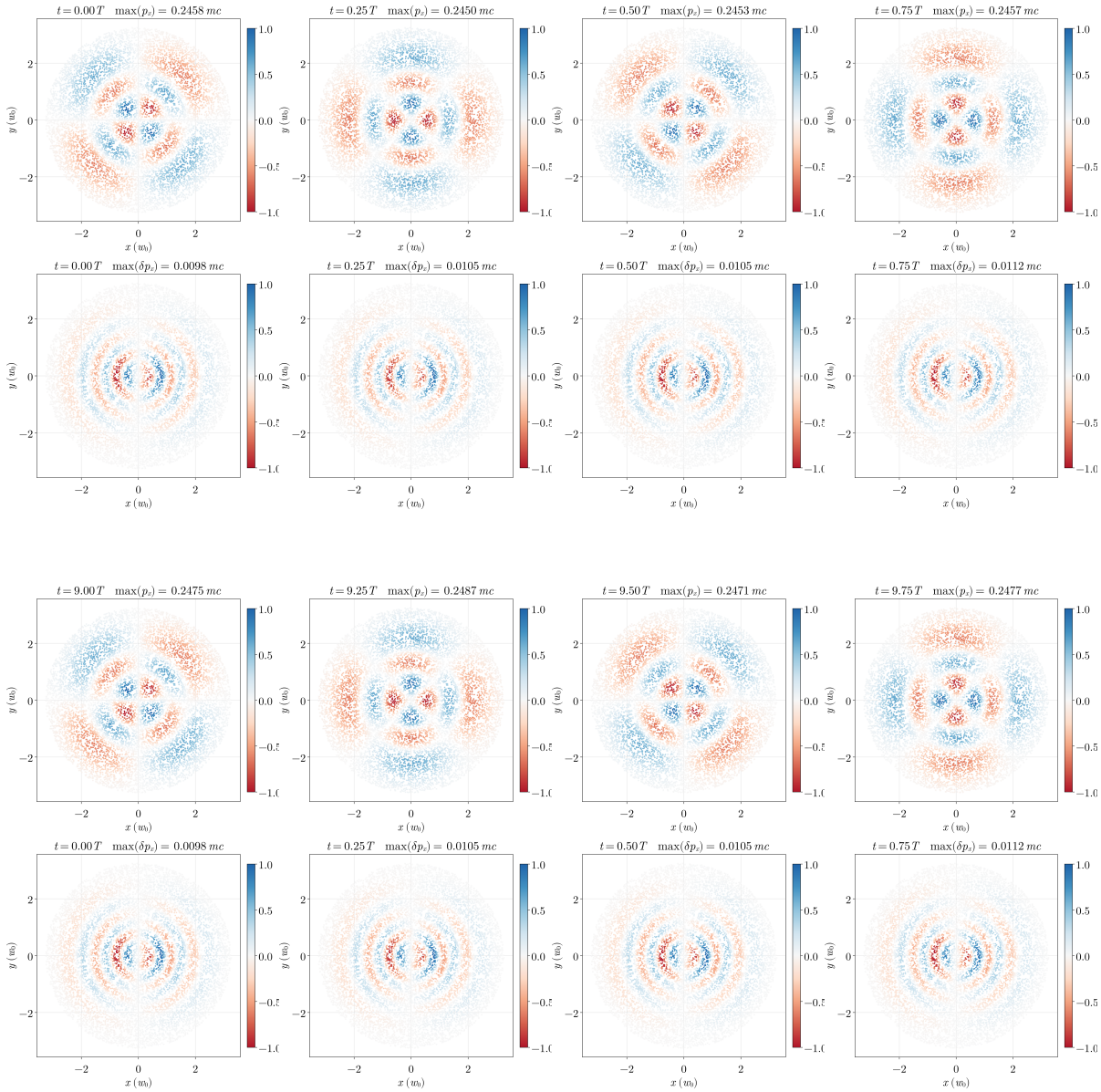


FIG. 3. Snapshots of  $p_x^{\text{exact}}$  (upper rows) and  $\delta p_x = p_x^{\text{exact}} - p_x^{\text{LPWA}}$  for each particle in a statistical ensemble of electrons in interaction with a LG beam with  $p_L = 2$ ,  $m_L = 2$ ,  $\xi_0 = 0.5$  for different times  $t \in (0, 10T)$  written on each graphic; the maximum value of  $|p_x|$  and respectively  $|\delta p_x|$  is written at every moment in the title of each graphic.

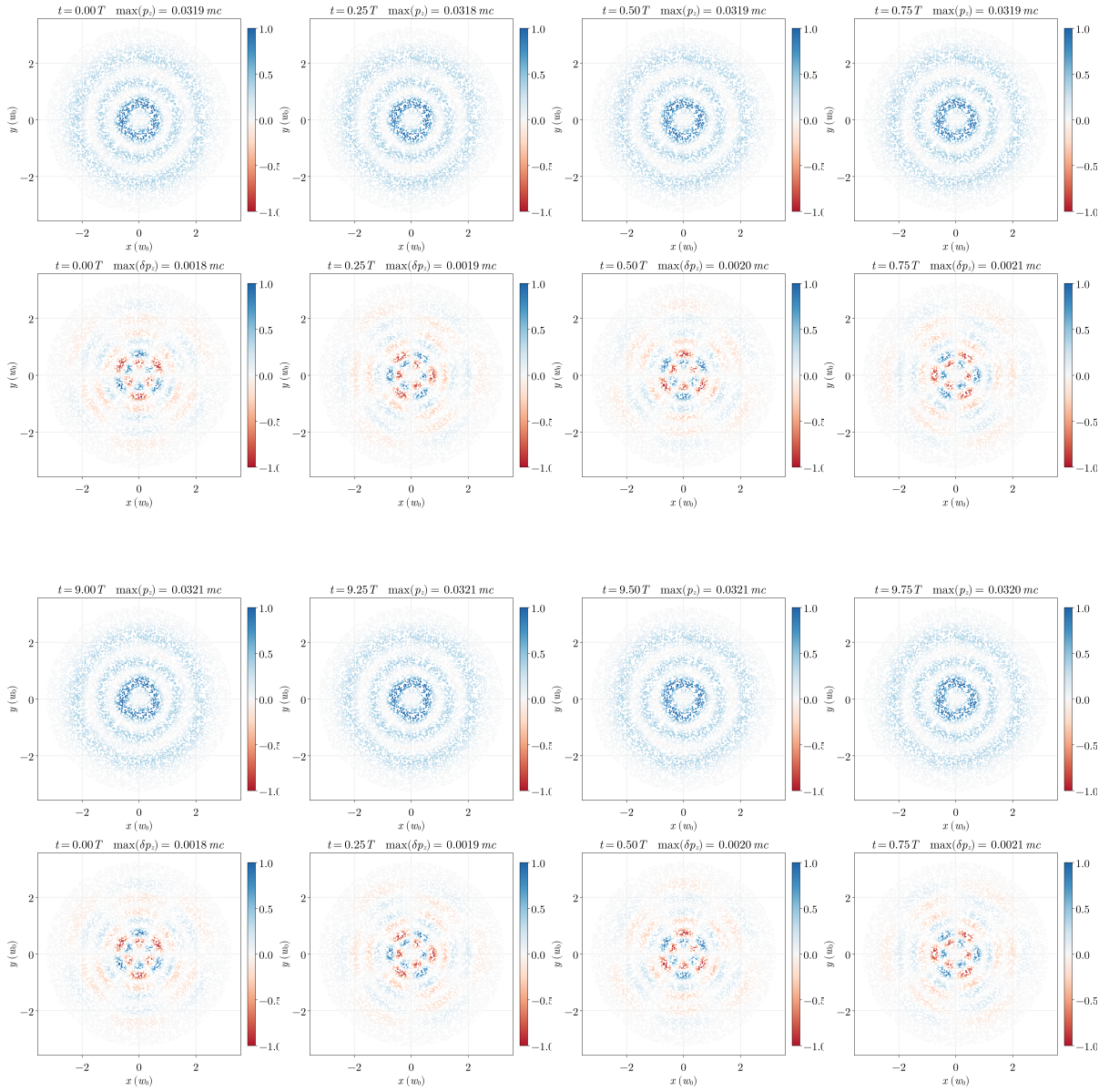


FIG. 4. Snapshots of  $p_z^{\text{exact}}$  (upper rows) and  $\delta p_z = p_z^{\text{exact}} - p_z^{\text{LPWA}}$  for each particle in a statistical ensemble of electrons in interaction with a LG beam with  $p_L = 2$ ,  $m_L = 2$ ,  $\xi_0 = 0.5$  for different times  $t \in (0, 10T)$  written on each graphic; the maximum value of  $|p_z|$  and respectively  $|\delta p_z|$  is written at every moment in the title of each graphic.

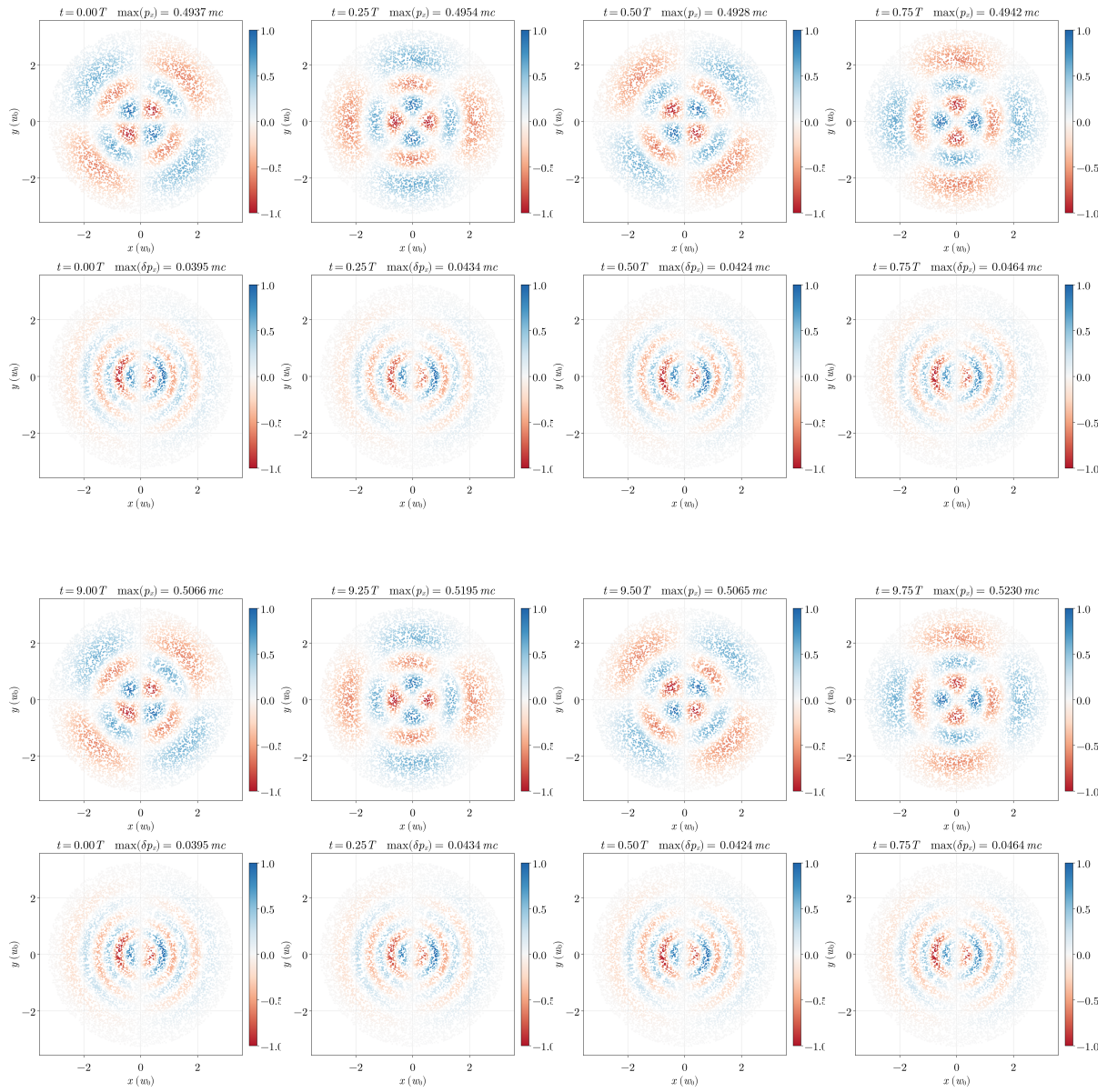
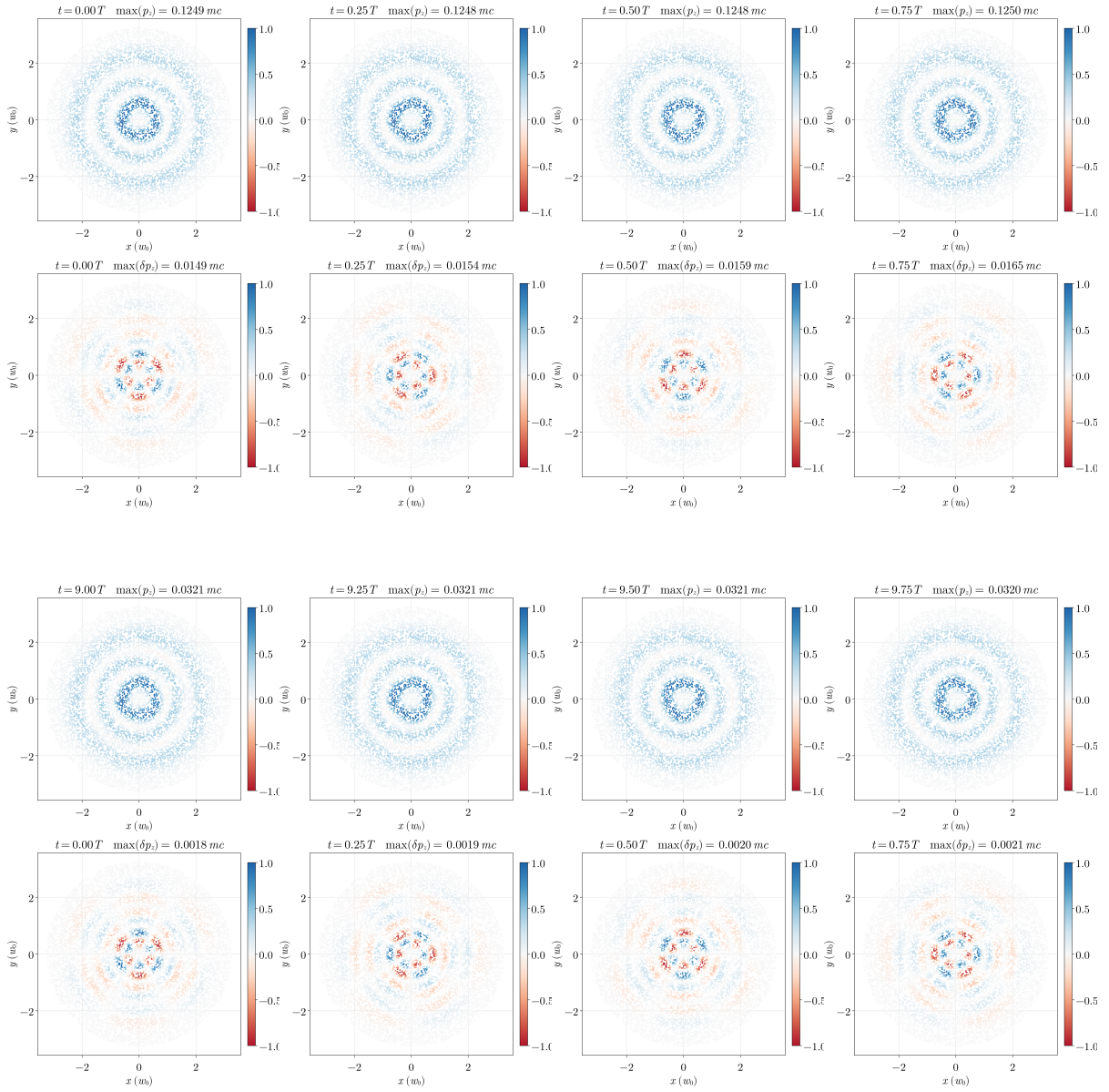


FIG. 5. The same as 3 but for  $\xi_0 = 1.0$

FIG. 6. The same as 4 but for  $\xi_0 = 1.0$ 

127

## II. THOMSON SCATTERING OF LAGUERRE GAUSS BEAMS

128

### A. Fourier analysis of the emitted fields - large distance approximation

129 Here we consider only the large distance approximation of the electromagnetic fields emitted by a particle of charge  
 130  $e_0$ , moving along the trajectory  $\mathbf{r}(t)$ , in the vicinity of the point  $\mathfrak{R}_0$  (here  $\mathfrak{R}_0$  is the initial position of the particle.)

$$\mathbf{E}(\mathbf{x}, t) = \frac{e_0}{4\pi\epsilon_0|\mathbf{x}_0|} \frac{\mathbf{n}_0 \times [(\mathbf{n}_0 - \boldsymbol{\beta}) \times \mathbf{a}]}{c^2(1 - \boldsymbol{\beta} \cdot \mathbf{n}_0)^3} \Big|_{t=t_r}, \quad \mathbf{B}(\mathbf{x}, t) = \frac{1}{c} \mathbf{n}_0 \times \mathbf{E}(\mathbf{x}, t) \quad (14)$$

131 where  $\mathbf{x}$  is the observation point,

$$\mathbf{x}_0 = \mathbf{x} - \mathfrak{R}_0, \quad \mathbf{n}_0 = \frac{\mathbf{x}_0}{|\mathbf{x}_0|} \quad (15)$$

132  $\boldsymbol{\beta}$  is the velocity measured in units of  $c$  and  $\mathbf{a}$  the particle acceleration. We define the temporal Fourier transform

$$\mathbf{E}(\mathbf{x}, k) = \frac{1}{\sqrt{2\pi}} \int_{-\infty}^{\infty} d(ct) \mathbf{E}(\mathbf{x}, t) e^{ik(ct)} = \frac{1}{\sqrt{2\pi}} \int_{-\infty}^{\infty} d(ct) \frac{q}{4\pi\epsilon_0|\mathbf{x}_0|} \frac{\mathbf{n}_0 \times [(\mathbf{n}_0 - \boldsymbol{\beta}) \times \mathbf{a}]}{c^2(1 - \boldsymbol{\beta} \cdot \mathbf{n}_0)^3} \Big|_{t=t_r} e^{ik(ct)} \quad (16)$$

133 and we use the retarded time as a integration variable

$$t = t_r + \frac{|\mathbf{x}_0 - \mathbf{r}_0|}{c} \approx t_r + \frac{|\mathbf{x}_0|}{c} - \frac{\mathbf{n}_0 \cdot \mathbf{r}_0}{c}, \quad dt = dt_r(1 - \boldsymbol{\beta} \cdot \mathbf{n}_{R_0}) \approx dt_r(1 - \boldsymbol{\beta} \cdot \mathbf{n}_0); \quad (17)$$

134 with these we obtain

$$\mathbf{E}(\mathbf{x}, k) = \frac{q}{4\pi\epsilon_0|\mathbf{x}_0|} \frac{1}{\sqrt{2\pi}} \int_{-\infty}^{\infty} d(ct_r) \frac{\mathbf{n}_0 \times [(\mathbf{n}_0 - \boldsymbol{\beta}) \times \mathbf{a}]}{c^2(1 - \boldsymbol{\beta} \cdot \mathbf{n}_0)^2} e^{ik((ct_r) + |\mathbf{x}_0| - \mathbf{n}_0 \cdot \mathbf{r}_0)} \quad (18)$$

135 Next we use the identity

$$\frac{d}{dt} \frac{\mathbf{n}_0 \times (\mathbf{n}_0 \times \boldsymbol{\beta})}{1 - \boldsymbol{\beta} \cdot \mathbf{n}_0} = \frac{1}{c(1 - \boldsymbol{\beta} \cdot \mathbf{n}_0)^2} [\mathbf{n}_0(\mathbf{n}_0 \cdot \mathbf{a}) - \mathbf{a} + \mathbf{a}(\boldsymbol{\beta} \cdot \mathbf{n}_0) - \boldsymbol{\beta}(\mathbf{n}_0 \cdot \mathbf{a})] = \frac{\mathbf{n}_0 \times [(\mathbf{n}_0 - \boldsymbol{\beta}) \times \mathbf{a}]}{c(1 - \boldsymbol{\beta} \cdot \mathbf{n}_0)^2} \quad (19)$$

136 and we write an equivalent form of the Fourier transform

$$\mathbf{E}(\mathbf{x}, k) = \frac{e_0}{4\pi\epsilon_0|\mathbf{x}_0|} \frac{1}{\sqrt{2\pi}} \int_{-\infty}^{\infty} d(ct_r) c \frac{d}{d(ct_r)} \left[ \frac{\mathbf{n}_0 \times (\mathbf{n}_0 \times \boldsymbol{\beta}(t_r))}{c(1 - \boldsymbol{\beta}(t_r) \cdot \mathbf{n}_0)} \right] e^{ik(ct_r + |\mathbf{x}_0| - \mathbf{n}_0 \cdot \mathbf{r}_0(t_r))} \quad (20)$$

137 After an integration by parts we obtain the well known formula [5]

$$\mathbf{E}(\mathbf{x}, k) = \frac{-ike_0 e^{ik|\mathbf{x}_0|}}{4\pi\epsilon_0|\mathbf{x}_0|} \frac{1}{\sqrt{2\pi}} \int_{-\infty}^{\infty} d(ct) [\mathbf{n}_0 \times (\mathbf{n}_0 \times \boldsymbol{\beta}(t))] e^{ik(ct - \mathbf{n}_0 \cdot \mathbf{r}_0(t))} \quad (21)$$

$$\mathbf{B}(\mathbf{x}, k) = \frac{1}{c} \mathbf{n}_0 \times \mathbf{E}(\mathbf{x}, k) \quad (22)$$

138

## B. The trajectory of a particle in a monochromatic field

139 Consider a particle, initially in the position

$$\mathbf{r}(0) = \mathfrak{R}_0 \quad (23)$$

140 in the  $Oxy$  plane. We denote by  $(\rho_0, \Phi_0)$  the cylindrical coordinates of the initial position of the particle and define

$$\mathbf{r}_0 = \mathbf{x} - \mathfrak{R}_0 \quad (24)$$

141 The particle interacts with an LG beam of not too large intensity, of indices  $(p_L, m_L)$ , the field is approximated as  
142 monochromatic, with a  $\rho_0$  dependent amplitude, and an initial phase  $m_L \Phi_0$ . Consider a plane wave monochromatic  
143 field of frequency  $\omega_L = ck_L$ , propagating along the  $Oz$  direction, described by the vector potential

$$\mathbf{A}(\phi) = A_0 [e_x \zeta_x \cos(k_L \phi - m_L \Phi_0) + e_y \zeta_y \sin(k_L \phi - m_L \Phi_0)], \quad \zeta_x^2 + \zeta_y^2 = 1, \quad \phi = ct - z \quad (25)$$

144 Consider a charged particle, of charge  $e_0$ , in the presence of the field with the initial conditions

$$\mathbf{p}_i = \mathbf{p}_0, \quad \mathbf{A}(\mathbf{r}_i, t_i) = \mathbf{A}_0 \quad (26)$$

145 i.e. the initial momentum is  $\mathbf{p}_0$  and the value of the vector potential at the initial position of the particle is  $\mathbf{A}_0$ . With  
146 these, the particle trajectory  $\mathbf{r}_0(t)$  can be written as an analytic function of the variable  $\chi = ct - z_0$

$$\begin{aligned} \mathbf{r}_{0\perp}(\chi) &= \int_{ct_i - z_i}^{\chi} d\phi \frac{\mathbf{p}_{0\perp} - e\mathbf{A}(\phi)}{n_L \cdot \mathbf{p}_0}, \quad z_0(\chi) = \int_{ct_i - z_i}^{\chi} d\phi F(\phi), \quad \chi = ct - z_0 \\ F(\chi) &= \frac{e^2 \mathcal{A}^2(\chi)}{2(n_L \cdot \mathbf{p}_0)^2} + \frac{p_{0z}}{n_L \cdot \mathbf{p}_0}, \quad e^2 \mathcal{A}^2(\chi) = e^2 \mathbf{A}^2(\chi) - 2e\mathbf{A}(\chi) \cdot \mathbf{p}_{0\perp}, \quad n_L = (1, \mathbf{e}_z) \end{aligned} \quad (27)$$

147 We discuss the particular case:

$$t_i = 0, \quad z_i = 0, \quad \mathbf{p}_0 = 0 \quad (28)$$

148 and use the notation

$$\xi_0 = \frac{-e_0 A_0}{m_e c}. \quad (29)$$

149 The trajectory can be written as

$$\mathbf{r}_{0\perp}(\chi) = \frac{\xi_0}{k_L} [\mathbf{e}_x \zeta_x \sin(k_L \chi + m_L \Phi_0) - \mathbf{e}_y \zeta_y \cos(k_L \chi + m_L \Phi_0)] \quad (30)$$

$$z_0(\chi) = \frac{\xi_0^2}{4} \left[ \chi + \frac{(\zeta_x^2 - \zeta_y^2) \sin(2k_L \chi + 2m_L \Phi_0)}{2k_L} \right] - z_{in}, \quad z_{in} = \frac{\xi_0^2}{4} \frac{\zeta_x^2 - \zeta_y^2}{2k_L} \sin(2m_L \Phi_0). \quad (31)$$

150 We also write the velocity of the particle as a function of  $\chi$

$$\boldsymbol{\beta} = \frac{d\mathbf{r}(\chi)}{d\chi} \frac{d\chi}{d(ct)} = \frac{d\mathbf{r}(\chi)}{d\chi} (1 - \beta_z) \quad (32)$$

$$\beta_z = \frac{\xi_0^2}{4} [1 + (\zeta_x^2 - \zeta_y^2) \cos(2k_L \chi - 2m_L \Phi_0)] (1 - \beta_z) \quad (33)$$

151 which can be put in an equivalent form

$$\beta_z(\chi) = \frac{F(\chi)}{1 + F(\chi)}, \quad F(\chi) = \frac{\xi_0^2}{4} [1 + (\zeta_x^2 - \zeta_y^2) \cos(2k_L \chi - 2m_L \Phi_0)] \quad (34)$$

$$\boldsymbol{\beta}_\perp(\chi) = \xi_0 [\mathbf{e}_x \zeta_x \cos(k_L \chi - m_L \Phi_0) + \mathbf{e}_y \zeta_y \sin(k_L \chi - m_L \Phi_0)] \frac{1}{1 + F(\chi)}. \quad (35)$$

152

### C. The field emitted by a particle in an LG beam

153 Consider a particle, initially in the position

$$\mathbf{r}(0) = \mathfrak{R}_0 \quad (36)$$

154 in the  $Oxy$  plane. We denote by  $(\rho_0, \Phi_0)$  the cylindrical coordinates of the initial position of the particle.

155 The particle interacts with an LG beam of not too large intensity, of indices  $(p, m)$ . Then the trajectory of  
156 the particle can be approximated according to the formulas in the previous section, with an intensity parameter  $\xi$   
157 dependent on the radial coordinate  $\rho_0$ .

$$\mathbf{r}(t) - \mathfrak{R}_0 = \mathbf{r}_0(t)$$

$$\mathbf{r}_{0\perp}(\chi) = \frac{\xi(\varrho_0)}{k_L} [\mathbf{e}_x \zeta_x \sin(k_L \chi - m_L \Phi_0) - \mathbf{e}_y \zeta_y \cos(k_L \chi - m_L \Phi_0)] \quad (37)$$

$$z_0(\chi) = \frac{\xi^2(\varrho_0)}{4} \left[ \chi + \frac{(\zeta_x^2 - \zeta_y^2) \sin(2k_L \chi - 2m_L \Phi_0)}{2k_L} \right] + z_{in} \quad (38)$$

$$\beta_z(\chi) = \frac{F(\chi)}{1 + F(\chi)}, \quad \boldsymbol{\beta}_\perp(\chi) = \xi(\varrho_0) [\mathbf{e}_x \zeta_x \cos(k_L \chi - m_L \Phi_0) + \mathbf{e}_y \zeta_y \sin(k_L \chi - m_L \Phi_0)] \frac{1}{1 + F(\chi)} \quad (39)$$

$$F(\chi) = \frac{\xi^2(\varrho_0)}{4} [1 + (\zeta_x^2 - \zeta_y^2) \cos(2k_L \chi - 2m_L \Phi_0)] \quad (40)$$

158 We use the previous results in the expression of the emitted electric field

$$\mathbf{E}(\mathbf{x}, k) = \frac{-ik e_0 e^{ik|\mathbf{x}_0|}}{4\pi\epsilon_0 |\mathbf{x}_0|} \frac{1}{\sqrt{2\pi}} \int_{-\infty}^{\infty} d(ct) [\mathbf{n}_0 \times (\mathbf{n}_0 \times \boldsymbol{\beta}(t))] e^{ik(ct - \mathbf{n}_0 \cdot \mathbf{r}_0(t))} \quad (41)$$

159 In the previous integral we perform another change of variable from  $t$  to  $\chi = ct - z$ , using

$$d\chi = c(1 - \beta_z(\chi))dt = c \frac{1}{1 + F(\chi)} dt, \quad \rightarrow \quad dt = \frac{1}{c} d\chi(1 + F(\chi)) \quad (42)$$

160 is also convenient to redefine the velocity

$$\boldsymbol{\beta} = \frac{1}{1 + F(\chi)} \tilde{\boldsymbol{\beta}}(\chi) \quad (43)$$

$$\tilde{\boldsymbol{\beta}}_{\perp}(\chi) = \xi(\varrho_0) [\mathbf{e}_x \zeta_x \cos(k_L \chi - m_L \Phi_0) + \mathbf{e}_y \zeta_y \sin(k_L \chi - m_L \Phi_0)], \quad (44)$$

$$\tilde{\beta}_z(\chi) = F(\chi) = \frac{\xi^2(\varrho_0)}{4} [1 + (\zeta_x^2 - \zeta_y^2) \cos(2k_L \chi - 2m_L \Phi_0)] \quad (45)$$

161 and obtain the Fourier transform of the emitted electric field

$$\mathbf{E}(\mathbf{x}, k) = \frac{-ik\epsilon_0 e^{ik|\mathbf{x}_0|}}{4\pi\epsilon_0 |\mathbf{x}_0|} \frac{1}{\sqrt{2\pi}} \int_{-\infty}^{\infty} d\chi [\mathbf{n}_0 \times (\mathbf{n}_0 \times \tilde{\boldsymbol{\beta}}(\chi))] e^{ik(\chi + z(\chi) - \mathbf{n}_0 \cdot \mathbf{r}_0(\chi))} \quad (46)$$

162 and, denoting by  $\theta_0$ ,  $\phi_0$  the polar angles of  $\mathbf{n}_0$  and using  $\mathbf{n}_L = \mathbf{e}_z$  we have

$$z(\chi) - \mathbf{n}_0 \cdot \mathbf{r}_0(\chi) = \mathbf{n}_L \cdot \mathbf{r}_0(\chi) - \mathbf{n}_0 \cdot \mathbf{r}_0(\chi) = (\mathbf{n}_L - \mathbf{n}_0) \cdot \mathbf{r}_0(\chi) \quad (47)$$

163 Next we write the explicit form of  $(\mathbf{n}_L - \mathbf{n}_0) \cdot \mathbf{r}_0(\chi)$ ;

$$\begin{aligned} (\mathbf{n}_L - \mathbf{n}_0) \cdot \mathbf{r}_0(\chi) = & -\frac{\xi(\varrho_0)}{k_L} \sin \theta_0 \sqrt{\cos^2 \phi_0 \zeta_x^2 + \sin^2 \phi_0 \zeta_y^2} \\ & \times \left[ \sin(k_L \chi - m_L \Phi_0) \frac{\cos \phi_0 \zeta_x}{\sqrt{\cos^2 \phi_0 \zeta_x^2 + \sin^2 \phi_0 \zeta_y^2}} - \cos(k_L \chi - m_L \Phi_0) \frac{\sin \phi_0 \zeta_y}{\sqrt{\cos^2 \phi_0 \zeta_x^2 + \sin^2 \phi_0 \zeta_y^2}} \right] \end{aligned} \quad (48)$$

164 We introduce the notations:

$$\begin{aligned} n_L &= (1, \mathbf{n}_L) \equiv (1, \mathbf{e}_z), & n_0 &= (1, \mathbf{n}_0), & 1 - \cos \theta_0 &= n_L \cdot n_0, \\ \gamma_0 &= \arctan \left( \frac{\sin \phi_0 \zeta_y}{\cos \phi_0 \zeta_x} \right), & \Gamma_0 &= \frac{\xi(\varrho_0)}{k_L} \sin \theta_0 \sqrt{\cos^2 \phi_0 \zeta_x^2 + \sin^2 \phi_0 \zeta_y^2}, & \Delta_0 &= n_L \cdot n_0 \frac{\xi^2(\varrho_0)}{8k_L} (\zeta_x^2 - \zeta_y^2) \\ (1 - \cos \theta_0) z_{in} &= n_L \cdot n_0 \frac{\xi^2(\varrho_0)}{4} \frac{\zeta_x^2 - \zeta_y^2}{2k_L} \sin(2m_L \Phi_0) = Z_0 \end{aligned} \quad (49)$$

165 and we can write

$$\chi + (\mathbf{n}_L - \mathbf{n}_0) \cdot \mathbf{r}_0(\chi) = \chi \left( 1 + n_L \cdot n_0 \frac{\xi^2(\varrho_0)}{4} \right) - \Gamma_0 \sin(k_L \chi - m_L \Phi_0 - \gamma_0) + \Delta_0 \sin(2k_L \chi - 2m_L \Phi_0) + Z_0. \quad (50)$$

166 Using the Anger identity [6]

$$e^{iz \sin \phi} = \sum_{n=-\infty}^{\infty} e^{in\phi} J_n(z) \quad (51)$$

167 to expand the exponential in the expression (46) and we obtain

$$e^{ik(\phi + z(\phi) - \mathbf{n}_0 \cdot \mathbf{r}_0(\phi))} = e^{-ikZ_0} e^{ik\phi(1 + n_L \cdot n_0 \frac{\xi^2(\varrho_0)}{4})} \sum_{M=-\infty}^{\infty} e^{-iMk_L \phi} e^{iMm_L \Phi_0} \sum_{p=-\infty}^{\infty} e^{i(M+2p)\gamma_0} J_{M+2p}(k\Gamma_0) J_p(k\Delta_0) \quad (52)$$

168 We define a generalized Bessel function

$$\tilde{J}_M(k; \gamma_0, \Gamma_0, \Delta_0) = \sum_{p=-\infty}^{\infty} e^{i(M+2p)\gamma_0} J_{M+2p}(k\Gamma_0) J_p(k\Delta_0) \quad (53)$$

169 which depends on the argument  $k$  and the parameters  $\gamma_0, \Gamma_0, \Delta_0$ . Then the expansion (52) can be further written as

$$e^{ik(\chi+z(\chi)-\mathbf{n}_0 \cdot \mathbf{r}_0(\chi))} = e^{ik\chi(1+n_L \cdot \mathbf{n}_0 \frac{\xi^2(\varrho_0)}{4})} \sum_{M=-\infty}^{\infty} e^{-iMk_L\chi} e^{iMm_L\Phi_0 + ikZ_0} \tilde{J}_M(k; \gamma_0, \Gamma_0, \Delta_0) \quad (54)$$

170 Also the integrand in (46) can be written in the equivalent form

$$\begin{aligned} \mathbf{n}_0 \times (\mathbf{n}_0 \times \tilde{\beta}) &= \xi(\varrho_0) \left[ \nu_{0x} \frac{1}{2} \zeta_x \left( e^{i(k_L\phi - m_L\Phi_0)} + e^{-i(k_L\phi - m_L\Phi_0)} \right) + \nu_{0y} \frac{1}{2i} \zeta_y \left( e^{i(k_L\phi - m_L\Phi_0)} - e^{-i(k_L\phi - m_L\Phi_0)} \right) \right] \\ &\quad + \frac{\xi^2(\varrho_0)}{4} \nu_{0z} \left[ 1 + (\zeta_x^2 - \zeta_y^2) \cos(2k_L\phi - 2m_L\Phi_0) \right] \end{aligned} \quad (55)$$

$$\begin{aligned} &= \frac{\xi(\varrho_0)}{2} \nu_- e^{i(k_L\phi - m_L\Phi_0)} + \frac{\xi(\varrho_0)}{2} \nu_+ e^{-i(k_L\phi - m_L\Phi_0)} \\ &\quad + \frac{\xi^2(\varrho_0)}{4} \nu_{0z} \left[ 1 + \frac{(\zeta_x^2 - \zeta_y^2)}{2} e^{2i(k_L\phi - m_L\Phi_0)} + \frac{(\zeta_x^2 - \zeta_y^2)}{2} e^{-2i(k_L\phi - m_L\Phi_0)} \right], \\ \mathbf{n}_0 \times (\mathbf{n}_0 \times \mathbf{e}_{\{x,y,z\}}) &= \nu_{0\{x,y,z\}}, \quad \nu_{\pm} = \zeta_x \nu_{0x} \pm i\zeta_y \nu_{0y}, \quad (\nu_{\pm})^* = \nu_{\mp} \end{aligned} \quad (56)$$

171 With these the Fourier transform of the emitted electric field becomes

$$\mathbf{E}(\mathbf{x}, k) = \sum_{N=-\infty}^{\infty} \tilde{\mathbf{E}}_N(\mathbf{x}) \delta(k - N \frac{k_L}{\alpha}), \quad (57)$$

172 with

$$\begin{aligned} \tilde{\mathbf{E}}_N(\mathbf{x}; \varrho_0, \Phi_0) &= \frac{-ik_N e_0 e^{ik_N(|\mathbf{x}_0| + Z_0)}}{4\pi\epsilon_0 |\mathbf{x}_0| \alpha} \sqrt{2\pi} e^{iNm_L\Phi_0} \left[ \nu_+ \frac{\xi(\varrho_0)}{2} \tilde{J}_{N-1}(k_N; \gamma_0, \Gamma_0, \Delta_0) + \nu_- \frac{\xi(\varrho_0)}{2} \tilde{J}_{N+1}(k_N; \gamma_0, \Gamma_0, \Delta_0) + \right. \\ &\quad \left. \nu_{0z} \left( \frac{\xi^2(\varrho_0)}{4} \tilde{J}_N(k_N; \gamma_0, \Gamma_0, \Delta_0) + \frac{\xi^2(\varrho_0)}{8} (\zeta_x^2 - \zeta_y^2) \tilde{J}_{N-2}(k_N; \gamma_0, \Gamma_0, \Delta_0) + \frac{\xi^2(\varrho_0)}{8} (\zeta_x^2 - \zeta_y^2) \tilde{J}_{N+2}(k_N; \gamma_0, \Gamma_0, \Delta_0) \right) \right], \\ \alpha &= 1 + \frac{\xi^2(\varrho_0)}{4} \mathbf{n}_0 \cdot \mathbf{n}_L, \quad k_N = N \frac{k_L}{\alpha}; \end{aligned} \quad (58)$$

173 here we indicated explicitly the dependence on the cylindrical variables of the initial position of the electron  $\varrho_0, \varphi_0$ .

174 In the same approximation, the magnetic field is

$$\mathbf{B}(\mathbf{x}, k) = \frac{1}{c} \mathbf{n}_0 \times \mathbf{E}(\mathbf{x}, k) = \sum_{N=-\infty}^{\infty} \tilde{\mathbf{B}}_N(\mathbf{x}) \delta(k - N \frac{k_L}{\alpha}) \quad (59)$$

175 with

$$\begin{aligned} \tilde{\mathbf{B}}_N(\mathbf{x}; \varrho_0, \Phi_0) &= \frac{-ik_N e_0 e^{ik_N(|\mathbf{x}_0| + Z_0)}}{4\pi\epsilon_0 |\mathbf{x}_0| c\alpha} \sqrt{2\pi} e^{iNm_L\Phi_0} \left[ \mu_+ \frac{\xi(\varrho_0)}{2} \tilde{J}_{N-1}(k_N; \gamma_0, \Gamma_0, \Delta_0) + \mu_- \frac{\xi(\varrho_0)}{2} \tilde{J}_{N+1}(k_N; \gamma_0, \Gamma_0, \Delta_0) + \right. \\ &\quad \left. \mu_{0z} \left( \frac{\xi^2(\varrho_0)}{4} \tilde{J}_N(k_N; \gamma_0, \Gamma_0, \Delta_0) + \frac{\xi^2(\varrho_0)}{8} (\zeta_x^2 - \zeta_y^2) \tilde{J}_{N-2}(k_N; \gamma_0, \Gamma_0, \Delta_0) + \frac{\xi^2(\varrho_0)}{8} (\zeta_x^2 - \zeta_y^2) \tilde{J}_{N+2}(k_N; \gamma_0, \Gamma_0, \Delta_0) \right) \right], \\ \mathbf{e}_{\pm} &= \zeta_x \mathbf{e}_x \pm i\zeta_y \mathbf{e}_y \\ \nu_{\pm} &= \mathbf{n}_0 \times (\mathbf{n}_0 \times \mathbf{e}_{\pm}) = -\mathbf{n}_0 \times \mu_{\pm}, \quad \nu_z = \mathbf{n}_0 \times (\mathbf{n}_0 \times \mathbf{e}_z) = -\mathbf{n}_0 \times \mu_z \\ \mu_{\pm} &= \mathbf{n}_0 \times \nu_{\pm} = -\mathbf{n}_0 \times \mathbf{e}_{\pm}, \quad \mu_{0z} = \mathbf{n}_0 \times \nu_{0z} = -\mathbf{n}_0 \times \mathbf{e}_z \end{aligned} \quad (60)$$

176 From the previous results we obtain the frequency spectrum of the emitted radiation, consisting in equidistant lines  
177 given by the well known formula of non-linear Thomson scattering

$$\omega_N = ck_N = \frac{N\omega_L}{1 + \frac{\xi^2(\varrho_0)}{4} \mathbf{n}_0 \cdot \mathbf{n}_L} = \frac{N\omega_L}{1 + \frac{\xi^2(\varrho_0)}{4} (1 - \cos\theta_0)} \quad (61)$$

178 The previous result shows that if the retardation is included the emitted frequency depends on the direction through  
 179 the polar angle  $\theta_0$  of the direction of observation unity vector  $\mathbf{n}_0$  (15); however, we shall see that when the coherent  
 180 sum of the field emitted by the entire electron distribution, at large distance from the focal plane dependence is very  
 181 weak.

182 Properties of the generalized Bessel functions

$$\begin{aligned}\tilde{J}_M(k; \gamma_0, \Gamma_0, \Delta_0) &= \sum_{p=-\infty}^{\infty} e^{i(M+2p)\gamma_0} J_{M+2p}(k\Gamma_0) J_p(k\Delta_0) \\ \tilde{J}_{-M}(-k; \gamma_0, \Gamma_0, \Delta_0) &= \sum_{p=-\infty}^{\infty} e^{i(-M+2p)\gamma_0} J_{-M+2p}(-k\Gamma_0) J_p(-k\Delta_0) = \sum_{p=-\infty}^{\infty} e^{i(-M+2p)\gamma_0} J_{M-2p}(k\Gamma_0) J_{-p}(k\Delta_0) \\ &= \sum_{p=-\infty}^{\infty} e^{-i(M+2p)\gamma_0} J_{M+2p}(k\Gamma_0) J_p(k\Delta_0) = [\tilde{J}_M(k; \gamma_0, \Gamma_0, \Delta_0)]^*\end{aligned}\quad (62)$$

$$\begin{aligned}\tilde{J}_{-M}(-k; \gamma_0, \Gamma_0, \Delta_0) &= \sum_{p=-\infty}^{\infty} e^{i(-M+2p)\gamma_0} J_{-M+2p}(-k\Gamma_0) J_p(-k\Delta_0) = \sum_{p=-\infty}^{\infty} e^{i(-M+2p)\gamma_0} J_{M-2p}(k\Gamma_0) J_{-p}(k\Delta_0) \\ &= \sum_{p=-\infty}^{\infty} e^{-i(M+2p)\gamma_0} J_{M+2p}(k\Gamma_0) J_p(k\Delta_0) = [\tilde{J}_M(k; \gamma_0, \Gamma_0, \Delta_0)]^*\end{aligned}\quad (63)$$

183 Then we can easily prove that

$$\mathbf{E}_{-N}(\mathbf{x}) = (E_N(\mathbf{x}))^*, \quad \mathbf{B}_{-N}(\mathbf{x}) = (B_N(\mathbf{x}))^* \quad (64)$$

184

### 1. The case of circular polarization

185 In the case of circular polarization  $\zeta_x = \epsilon_L \zeta_y$  with  $\epsilon_L = \pm 1$  the previous results have a much simpler form; we have

$$\begin{aligned}\gamma_0 &\rightarrow \epsilon_L \phi_0, & \Gamma_0 &\rightarrow \bar{\Gamma}_0 = \frac{\xi(\varrho_0)}{\sqrt{2}k_L} \sin \theta_0, & \Delta_0 &= 0, & Z_0 &= 0 \\ \tilde{J}_M(k; \gamma_0, \Gamma_0, \Delta_0) &\rightarrow e^{iM\epsilon_L \phi_0} J_M(k\bar{\Gamma}_0)\end{aligned}\quad (65)$$

186 If  $\theta_0 \ll 1$ , considering the behavior of Bessel functions at low arguments, we can also approximate the Fourier  
 187 components of the electric and magnetic field as

$$\begin{aligned}\tilde{\mathbf{E}}_N(\mathbf{x}; \varrho_0, \Phi_0) &\rightarrow \frac{-ik_N e_0 e^{ik_N |\mathbf{x}_0|}}{4\pi\epsilon_0 |\mathbf{x}_0| \alpha} \sqrt{2\pi\nu_+} \frac{\xi(\varrho_0)}{2} e^{iNm_L \Phi_0} e^{i(N-1)\epsilon_L \phi_0} J_{N-1}(k_N \frac{\xi(\varrho_0)}{\sqrt{2}k_L} \sin \theta_0) = \\ &= e^{-iNm_L \Phi_0} e^{i(N-1)\epsilon_L \phi_0} e^{ik_N |\mathbf{x}_0|} \mathcal{E}_N(\mathbf{x}; \varrho_0, \Phi_0) \\ \tilde{\mathbf{B}}_N(\mathbf{x}; \varrho_0, \Phi_0) &\rightarrow \frac{1}{c} e^{iNm_L \Phi_0} e^{i(N-1)\epsilon_L \phi_0} \mathbf{n}_0 \times \mathcal{E}_N(\mathbf{x}; \varrho_0, \Phi_0)\end{aligned}\quad (66)$$

188 In the previous equation we introduced the notation

$$\mathcal{E}_N(\mathbf{x}; \varrho_0, \Phi_0) = \frac{-ik_N e_0}{4\pi\epsilon_0 |\mathbf{x}_0| \alpha} \sqrt{2\pi\nu_+} \frac{\xi(\varrho_0)}{2} J_{N-1}(k_N \frac{\xi(\varrho_0)}{\sqrt{2}k_L} \sin \theta_0) \quad (67)$$

189 that will be used in the next section.

190

## III. INTEGRATION OVER THE INITIAL ELECTRON DISTRIBUTION

191 We consider the case of a charge distributed uniformly with the charge density  $\sigma_0$  within a disk of radius  $\rho_m$  in  
 192 the plane  $Oxy$ , interacting with an  $LG$  beam. We assume that the beam intensity is low, such that the amplitude of  
 193 the oscillatory motion of the particle is low with respect to waist  $w_0$  of the external beam. we also assume that the  
 194 particles are initially at rest, in the focal plane  $Oxy$ .

195 The field emitted by this distribution will be calculated as the superposition of the fields emitted by the elementary  
 196 charge  $de_0 = \sigma_0 da$  in each area element  $da$  within the disk.

$$\mathbf{E}_{tot}(\mathbf{x}, t) = \int_{\Sigma} da \mathbf{E}(\mathbf{x}, t) \quad (68)$$

197 and the Fourier transform becomes

$$\mathbf{E}_{tot}(\mathbf{x}, \omega) = \sum_{N=-\infty}^{\infty} \tilde{\mathbf{E}}_{N,tot}(\mathbf{x}, \omega), \quad \tilde{\mathbf{E}}_{N,tot}(\mathbf{x}) = \int_0^{\rho_m} d\rho_0 \rho_0 \int_0^{2\pi} d\Phi_0 \tilde{\mathbf{E}}_N(\mathbf{x}; \rho_0, \Phi_0) \delta(\omega - \omega_N) \quad (69)$$

198 and  $\omega_N$  is given by Eq. (61). Similarly, the Fourier transform of the total magnetic field radiated is

$$\mathbf{B}_{tot}(\mathbf{x}, \omega) = \sum_{N=-\infty}^{\infty} \tilde{\mathbf{B}}_{N,tot}(\mathbf{x}), \quad \tilde{\mathbf{B}}_{N,tot}(\mathbf{x}) = \int_0^{\rho_m} d\rho_0 \rho_0 \int_0^{2\pi} d\Phi_0 \tilde{\mathbf{B}}_N(\mathbf{x}; \rho_0, \Phi_0) \delta(\omega - \omega_N) \quad (70)$$

199 In the equations above  $\tilde{\mathbf{E}}_N$ ,  $\tilde{\mathbf{B}}_N$  are defined in Eqs. (57,59), where the electron charge  $e_0$  must be replaced by the  
200 surface charge density  $\sigma_0$  and  $\omega_N$  is a function of  $\rho_0$ ,  $\Phi_0$  through the angle  $\theta_0$  (see Eq. (61). If we consider only the  
201 scattering at very small angles ( $\theta_0 \ll 1$ ) and  $\xi_0 \leq 1$  then  $\omega_N$  can be written as

$$\omega_N \approx N\omega + \epsilon(\rho_0, \Phi_0), \quad \epsilon(\rho_0, \Phi_0) \ll 1 \quad (71)$$

202 Then we define the  $N$  th Fourier component of the total electric or magnetic field field as an integral over a small  
203 interval  $\Delta\omega \ll \omega_L$

$$\begin{aligned} \mathbf{E}_{N,tot}(\mathbf{x}) &\equiv \int_{N\omega_L - \Delta\omega/2}^{N\omega_L + \Delta\omega/2} d\omega \mathbf{E}_{N,tot}(\mathbf{x}; \rho_0, \Phi_0) = \int_0^{\rho_m} d\rho_0 \rho_0 \int_0^{2\pi} d\Phi_0 \tilde{\mathbf{E}}_N(\mathbf{x}; \rho_0, \Phi_0) \\ \mathbf{B}_{N,tot}(\mathbf{x}) &\equiv \frac{1}{c} \int_0^{\rho_m} d\rho_0 \rho_0 \int_0^{2\pi} d\Phi_0 \left( \mathbf{n}_0 \times \tilde{\mathbf{E}}_N(\mathbf{x}; \rho_0, \Phi_0) \right) \end{aligned} \quad (72)$$

204 In the expression of  $\tilde{\mathbf{E}}_N$  in the previous equations  $k$  must be replaced by  $k_N$  calculated according to the formula (58).

### 205 A. Analytical estimation of the phase of the emitted field in the circular polarization case

206 We consider the expression of the total emitted electric field of given harmonic index  $N$  (72)

$$\tilde{\mathbf{E}}_{N,tot}(\mathbf{x}) = \int_0^{\rho_m} d\rho_0 \rho_0 \int_0^{2\pi} d\Phi_0 \tilde{\mathbf{E}}_N(\mathbf{x}; \rho_0, \Phi_0) \quad (73)$$

207 and use here the approximation of  $\tilde{\mathbf{E}}_N$  (66)

$$\tilde{\mathbf{E}}_{N,tot}(\mathbf{x}) = \int_0^{\rho_m} d\rho_0 \rho_0 \int_0^{2\pi} d\Phi_0 e^{iN m_L \Phi_0} e^{i(N-1)\epsilon_L \phi_0} e^{ik_N |\mathbf{x}_0|} \mathcal{E}_N(\mathbf{x}; \rho_0, \Phi_0) \quad (74)$$

208 Next we analyze the integral over  $\Phi_0$ ; let us denote the cylindrical coordinates of the observation point by  $(\varrho, \Phi, Z)$

$$\mathbf{x} = \varrho \cos \Phi \mathbf{e}_x + \varrho \sin \Phi \mathbf{e}_y + Z \mathbf{e}_z \quad (75)$$

209 In a typical calculation  $Z$  is fixed and  $\varrho$ ,  $\Phi$  changes (we record the radiation on a screen perpendicular on the beam  
210 propagation direction at the distance  $Z$  from the focal plane). The distance  $|\mathbf{x}_0|$  is a function of  $\varrho_0$ ,  $\Phi_0$

$$|\mathbf{x}_0|(\varrho_0, \Phi_0) = \sqrt{(\varrho \cos \Phi - \varrho_0 \cos \Phi_0)^2 + (\varrho \sin \Phi - \varrho_0 \sin \Phi_0)^2 + Z^2} \quad (76)$$

211 and  $e^{iN k_L |\mathbf{x}_0|}$  is a very fast oscillating function; we use the stationary phase method for estimating the integral over  
212  $\Phi_0$ . We use the general formula [7]

$$\mathcal{I}_{\Phi_0} = \int d\Phi_0 e^{if(\Phi_0)} g(\Phi_0) \approx \sum_{y_0} \sqrt{\frac{2\pi}{|f''(y_0)|}} g(y_0) e^{if(y_0) + i\sigma \frac{\pi}{4}} \quad (77)$$

213 where  $y_0$  are the stationary points of  $f(\Phi_0)$

$$f'(y_0) = 0 \quad (78)$$

214 and  $\sigma$  is the sign of the second derivative  $f''(y_0)$

215 In our case

$$f(\Phi_0) = k_N |\mathbf{x}|_0(\varrho_0, \Phi_0) \quad (79)$$

216 and its derivative is

$$f'(\Phi_0) = -\frac{k_N \varrho \varrho_0 \sin(\Phi - \Phi_0)}{\sqrt{\varrho^2 + Z^2 + \varrho_0^2 - 2\varrho\varrho_0 \cos(\Phi - \Phi_0)}} \quad (80)$$

217 whose zeroes are

$$\Phi_0^{(1)} = \Phi, \quad \Phi_0^{(2)} = \Phi + \pi \quad (81)$$

218 and the integral over  $\Phi_0$  becomes

$$\begin{aligned} \mathcal{I}_{\Phi_0} &= e^{i(m_L N \Phi + \epsilon_L (N-1)\Phi)} \mathbf{h}(\mathbf{x}; \rho_0), \\ h(\mathbf{x}; \varrho_0) &= \sqrt{2\pi i} \left[ e^{iNk_L \sqrt{Z^2 + (\varrho - \varrho_0)^2}} \mathcal{E}(\mathbf{x}; \varrho_0, \Phi) \sqrt{\frac{\sqrt{Z^2 + (\varrho - \varrho_0)^2}}{Nk_L \varrho \varrho_0}} \right. \\ &\quad \left. - i(-1)^{Nm_L} e^{iNk_L \sqrt{Z^2 + (\varrho + \varrho_0)^2}} \mathcal{E}(\mathbf{x}; \varrho_0, \Phi + \pi) \sqrt{\frac{\sqrt{Z^2 + (\varrho + \varrho_0)^2}}{Nk_L \varrho \varrho_0}} \right] \end{aligned} \quad (82)$$

219 With these the expression of the total electric field measured in  $\mathbf{x}$  is

$$\tilde{\mathbf{E}}_{N,tot}(\mathbf{x}) = e^{i(m_L N \Phi + \epsilon_L (N-1)\Phi)} \int_0^{\rho_m} d\varrho_0 \varrho_0 \mathbf{h}(\mathbf{x}; \varrho_0) \quad (83)$$

220 whose dependence on  $\Phi$  is of the form

$$\mathbf{E}_{N,tot}(\mathbf{x}) \sim e^{iq\Phi}, \quad q = Nm_L + (N-1)\epsilon_L \quad (84)$$

221 Finally, we can estimate the behavior of the remaining integral over  $\varrho_0$ ; we write the function  $h(\varrho_0)$  as

$$h(\mathbf{x}, \varrho_0) = e^{iNk_L \sqrt{Z^2 + (\varrho - \varrho_0)^2}} \mathbf{h}_1(\mathbf{x}; \varrho_0) + e^{iNk_L \sqrt{Z^2 + (\varrho + \varrho_0)^2}} \mathbf{h}_2(\mathbf{x}, \varrho_0) \quad (85)$$

222 where  $\mathbf{h}_i(\varrho; \varrho_0)$  can be identified from the comparison with 82. In the integral over  $\varrho_0$  the two exponential functions  
 223  $e^{iNk_L \sqrt{Z^2 + (\varrho \pm \varrho_0)^2}}$  are, again, fast oscillating; from them, only  $e^{iNk_L \sqrt{Z^2 + (\varrho - \varrho_0)^2}}$  has a stationary point at  $\varrho_0 = \varrho$ , if  
 224  $\varrho \leq \varrho_m$ , with  $\varrho_m$  the upper limit of integral. As a consequence, if  $\rho \gtrsim \mathcal{O}(\varrho_m)$  the integral over  $\varrho_0$  depends slowly on  
 225  $\varrho$ , while for  $\varrho \lesssim \mathcal{O}(\varrho_m)$  the result is a fast oscillating function of  $\varrho$ .

- 
- 226 [1] P.-V. Toma, S. Micuța-Câmpeanu, M. Boca, A. Nicolin, and V. Băran, Scaling properties of angular momentum  
 227 transfer to charged particles under Laguerre-Gauss laser pulse, AIP Conference Proceedings **2843**, 020005 (2023),  
 228 [https://pubs.aip.org/aip/acp/article-pdf/doi/10.1063/5.0150590/18056737/020005\\_1\\_5.0150590.pdf](https://pubs.aip.org/aip/acp/article-pdf/doi/10.1063/5.0150590/18056737/020005_1_5.0150590.pdf).  
 229 [2] M. Dondera, Electrons in twisted fields and ponderomotive effects, JOURNAL OF PHYSICS B-ATOMIC MOLECULAR  
 230 AND OPTICAL PHYSICS **53**, 10.1088/1361-6455/ab678e (2020).  
 231 [3] A. Siegman, *Lasers* (University Science Books, 1986).  
 232 [4] M. B. Boca and V. Florescu, Thomson and compton scattering with an intense laser pulse, The European Physical Journal  
 233 D **61**, 449 (2011).  
 234 [5] J. D. Jackson, *Classical electrodynamics*, 3rd ed. (Wiley, New York, NY, 1999).  
 235 [6] H. Bateman and A. Erdelyi, *Higher transcendental functions*, California Institute of technology. Bateman Manuscript project  
 236 (McGraw-Hill, New York, NY, 1955).  
 237 [7] J. McClure and R. Wong, Multidimensional stationary phase approximation: boundary stationary point, Journal of Com-  
 238 putational and Applied Mathematics **30**, 213 (1990).